SIEMENS

# MReadings: MR in RT

Contributions from our MAGNETOM users

siemens.com/magnetom-world-rt


U.S.
Edition

MR compatible laser bridge (optional)
RT Dot Engine with optimized RT protocols for consistent scans
Tim 4G flexible coils for excellent image quality and bridges for proper positioning
RT compatible indexed flat table tops and high accuracy table (z-positioning accuracy ± 0.5 mm)

# Dear Reader,

Trends in modern radiation therapy point towards hypofractionated and highly precise treatments. Curative intent is becoming the goal of more and more treatments. These advancements drive the need for more advanced imaging. Indeed, according to a US survey conducted in 2014 [1], every fourth treatment plan used PET images and every fifth plan involved MR images – a four-fold increase in only seven years.

Following the rapid adoption of MRI in radiation therapy, Siemens has developed tailored solutions that also address those departments that have traditionally used CT imaging alone. This issue of the MReadings, aims to increase the peer-to-peer exchange of practices and to demonstrate how MAGNETOM users around the world are tackling the challenges posed by the introduction of MRI in the radiotherapy routine.

## Practical implementation of MRI in the workflow

Even in the past, institutions such as the Liverpool Cancer Therapy Centre in Sydney, Australia, relied heavily on local radiology scanners to access MR images for RT planning. In the first article of this issue, Liney et al. describe their initial experience with a dedicated installation of a 3T MAGNETOM Skyra for exclusive use in radiotherapy, and how they implemented MR-based planning into their clinical practice.

A prerequisite for the proper integration of MR into RT workflows is the ability to generate MR scans in the treatment position. In the second article, Koch et al. give hands-on guidance on how to set up patients with support devices, such as an MR compatible flat indexed tabletop and coils suitable for imaging in the treatment position.

In addition to these hardware components, Siemens Healthcare recently introduced a dedicated imaging workflow for Radiation Therapy (RT), the RT Dot Engine, which is described by my colleagues Thoermer and Requardt in the third article. Both the accessories for patient positioning as well as the RT Dot Engine are included in our dedicated MAGNETOM RT Pro edition for the MAGNETOM Aera 1.5T and the MAGNETOM Skyra 3T.

## Clinical application in external beam radiotherapy

Further evidence has been published in the scientific literature [2, 3].

## Quality assurance and management of spatial accuracy

Before introducing MRI in clinical routine, physicists will look into commissioning the system and verifying its geometric performance in order to ensure a high degree of accuracy. A variety of our systems are fitted with a higher order shim, which affects the resulting image quality. More information about magnet homogeneity (Figure 2) and shimming can be found in the white paper by Blasche and Fischer [7]. Siemens also proposes a set of QA recommendations, based on the ACR phantom (Figure 3) [8].

In this section, Balter et al., Stanescu and Jaffray, as well as Paulson focus on these topics, discuss the impact of subject-induced susceptibility on distortions and share their methods for comprehensive acceptance testing and quality assurance.

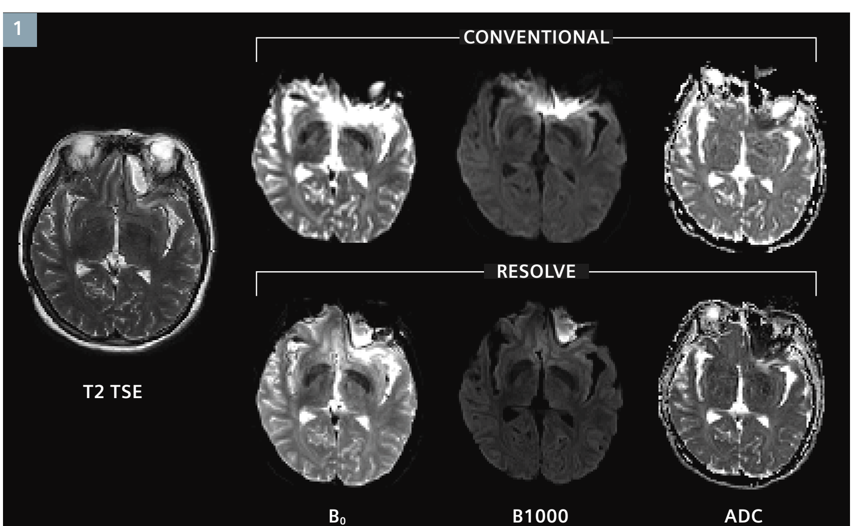


1 While spatial integrity of the conventionally acquired DWI scans often is compromised by susceptibility artifacts (caused by dental metal implants* in the case shown here), images acquired with the readout segmented DWI technique result in significantly reduced artifacts and superior spatial integrity.
*Images courtesy of Tongji Hospital, Wuhan, China.*

*The MRI restrictions (if any) of the metal implant must be considered prior to patient undergoing MRI exam. MR imaging of patients with metallic implants brings specific risks. However, certain implants are approved by the governing regulatory bodies to be MR conditionally safe. For such implants, the previously mentioned warning may not be applicable. Please contact the implant manufacturer for the specific conditional information. The conditions for MR safety are the responsibility of the implant manufacturer, not of Siemens.

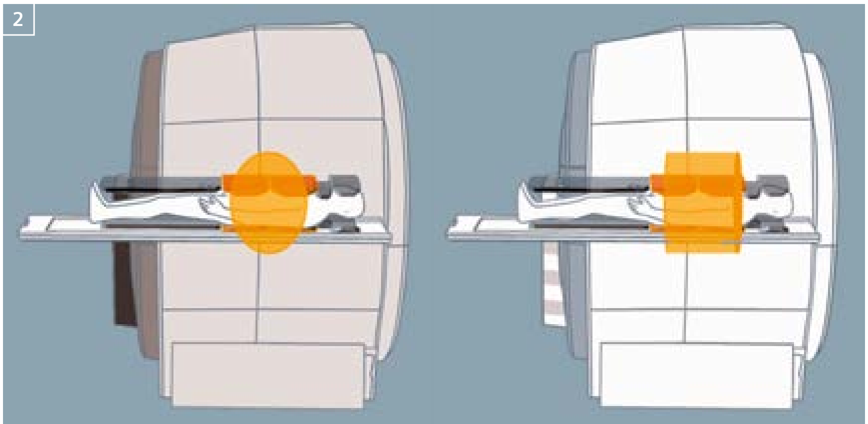

2 Visualization of the imaging volumes of a conventional magnet with spherical / ellipsoid volume (left) vs. TrueForm Magnet Design with a cylindrical volume (right).

3 Vertical setup of the ACR phantom in the scanner bore for quality assurance testing of geometric distortions.

I would like to thank all the authors publishing in this issue for sharing their expertise and enthusiasm with other MAGNETOM users. For those of you new to MRI in radiation therapy, I strongly encourage you to visit our online training and learn more about this exciting world at http://www.healthcare.siemens.com/radiation-oncology/imaging/magnetic-resonance/mri-training#webfeature

I wish you an enjoyable read!

Elena Nioutsikou
*Global Product Marketing Manager Imaging in RT*


### References

1. 2014 Radiation Therapy Market Summary Report. IMV 2014.
2. Quantitative evaluation of diffusion-weighted imaging techniques for the purposes of radiotherapy planning in the prostate G P Liney et al BJR 2015.
3. Readout-segmented echo-planar diffusion-weighted imaging improves geometric performance for image-guided radiation therapy of pelvic tumors. Foltz et al Radiother Oncol (2015).
4. Giese A, Westphal M. Glioma invasion in the central nervous system. Neurosurgery 1996 39(2):235-50.
5. https://www.embracestudy.dk/
6. EMBRACE: intErnational study on MRI guided BRachytherapy in locally Advanced CErvical cancer: Small changes, big improvements. European Journal of Cancer. 2013;49:5.
7. Siemens Healthcare GmbH white paper. Magnet Homogeneity and Shimming. Mathias Blasche and Daniel Fischer. 2015 Downloadable at the MAGNETOM World RT: siemens.com/magnetom-world-rt
8. Siemens Healthcare GmbH white paper. MRI Geometric Distortion QA. Nina Niebuhr 2014. Downloadable at the MAGNETOM World RT: www.siemens.com/magnetom-world-rt

# Content





[1] Radiotherapy planning where MR data is the only imaging information is ongoing research. The concepts and information presented in this article are based on research and are not commercially available. Its future availability cannot be ensured.

# A Dedicated MRI Scanner for Radiotherapy Planning: Early Experiences

Gary Liney[1, 2]; Robba Rai[1]; Lois Holloway[1]; Shalini Vinod[1]

[1] Liverpool Cancer Therapy Centre, Sydney, Australia
[2] Ingham Institute for Applied Medical Research, Sydney, Australia

## Introduction

The last decade has seen a dramatic increase in the use of MRI for radiotherapy planning. MRI has a number of advantages for the simulation of treatment plans, over the current gold standard of computed tomography (CT); Its excellent and variable soft-tissue contrast has been shown to improve the delineation accuracy of both the tumor and surrounding organs-at-risk; a range of functional techniques are able to measure and display tumor physiology in the same examination, potentially revealing sub-regions that could receive a boost in radiation dose; and finally, the absence of ionising radiation means the patient may be scanned any number of times before, during and after treatment, giving the clinician the ability to assess and adapt plans on an individual basis.

## MR-simulator

In common with most radiotherapy centres, our department at Liverpool Cancer Therapy Centre (LCTC), located


1

The 3 Tesla MAGNETOM Skyra MR-Simulator at Liverpool CTC, in south western Sydney, Australia. The 30 Gauss line can be seen marked on the floor which serves to emphasise this inner controlled area for the majority of our staff who have not previously worked in MRI. The object on the bed is our 3D volumetric distortion test phantom.



2 Photographs showing the RF coil set-up used in head and neck planning scans. **(2A)** Two small flexible coils are placed laterally around the fixation shell using two coil supports. **(2B)** The 18-channel body array is connected to one of the available ports at the bottom of the table using a long cable.

in south western Sydney, relied heavily on local radiology scanners to provide MR images. This often meant a compromise in image protocol and the limited availability of these busy scanners restricted our patient throughput and any opportunity for further development. However, in August 2013, as part of a wider investment in MRI, which will also see the Australian MR-Linac program on site, we installed our own dedicated system for the exclusive use of radiotherapy patients to provide MR-based treatment simulation scans. This scanner is a wide-bore 3 Tesla MAGNETOM Skyra with XQ gradients and 64-channel RF architecture and was purchased with the latest suite of functional imaging sequences. Our MR-Simulator (MR-sim), shown in Figure 1, is configured with a number of radiotherapy-specific features in mind including in-room lasers (as on a CT-simulator), flat indexed table top and a range of RF coils suitable for optimum imaging with the patients in the treatment position. The field strength was chosen with aspirations of incorporating functional studies into future clinical practice.

Over the last 12 months or so, our small but dedicated team has climbed a steep learning curve and implemented MR-based planning successfully into clinical practice for a variety of tumor sites. This process began even before the installation and acceptance testing of the system, with in-house safety and educational training being implemented for all radiotherapy and physics staff connected with MRI. Under normal operation, scanning is performed by our lead MR radiographer and one of a small number of specialist radiotherapists who are rotated through MR-Sim. Additional support is provided by the lead MR physicist and a radiologist. By preserving a significant portion of scan time during the week for research – one of the many advantages of having our own system – we have also been able to develop a number of studies that are beginning to explore the use of functional information and motion evaluation in treatment planning. This article serves as a brief illustration of how we are using this system in practice.

The vast majority of our workload requires MRI to be registered to CT for the electron density information needed in the dose calculation. To facilitate this, we image our patients in the treatment position and take advantage of the RF coils we have available. A good example of this is in head and neck tumors were patients lie on a flat table top and are imaged in a fixation shell placed over their head and shoulders which is attached to the table. Previous attempts to cater for this equipment on other scanners were compromised either due to a narrower 60 cm bore or unsuitable RF coils. On the MR-Sim we take advantage of the in-built 32-channel RF coil under the flat table-top and use this in conjunction with two laterally positioned 4-channel flexible coils attached to a supporting bridge. More recently we have been able to add an 18-channel body array connected at the foot of the table by a long cable (Fig. 2). This gives us vastly improved signal-to-noise ratio (SNR) and greater coverage compared to what had previously been possible as shown in Figure 3.

## Imaging details

In working up our protocols, we have had to consider the specific requirements of MR-simulation, which is often quite different from standard diagnostic procedure [1]. Geometric distortion is something we have to be especially mindful of. For radial distances less than 15 cm from isocentre (i.e. up to 30 cm FOV), system distortions caused by non uniformity in $B_0$ and non linearity of the gradients are within our tolerance, and the dominant contribution is instead

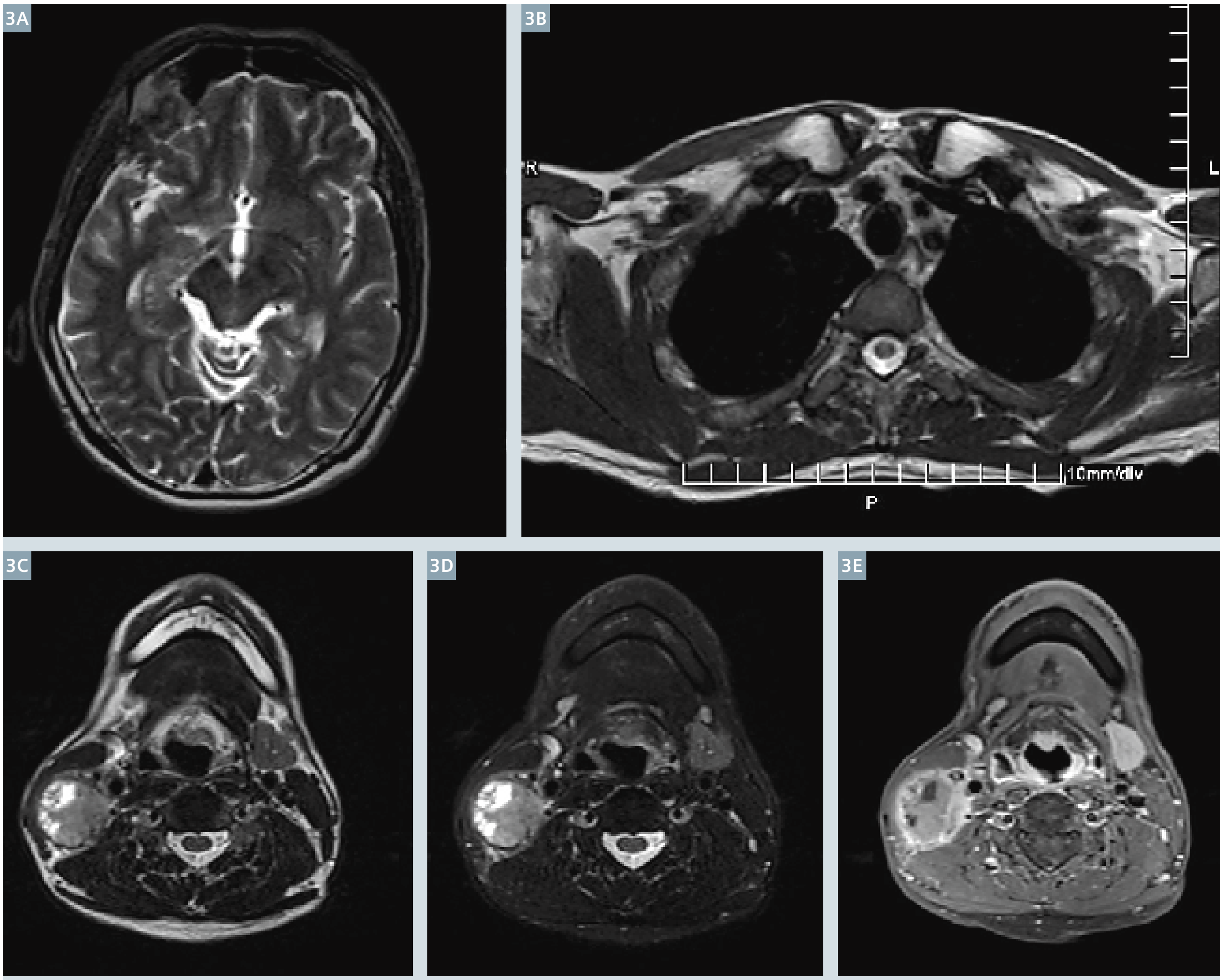


3 Example images acquired in a head and neck tumor patient. Figures **3A and B** serve to illustrate the image quality and coverage obtained using dedicated RF coils which extend from midbrain down to sternal notch. The bottom images show a slice taken through the tumor using **(3C)** Dixon T2w in-phase, **(3D)** water-only and **(3E)** Dixon T1w water-only post-contrast.

from chemical shift and magnetic susceptibility within the patient. These effects can be mitigated by use of high receiver bandwidths which we set to 440 Hz/pixel or greater. The large coverage that is required for planning creates long scan times compared to diagnostic practice and we rely heavily on iPAT technology to keep these down to an acceptable level. Nevertheless, these scan times inevitably result in some organ motion and we have found BLADE to be useful in reducing artifacts for example from bladder filling. One of our current studies is comparing the image quality of this radial *k*-space technique against the administration of anti-peristaltic agents and normal cartesian acquisition as shown in Figure 4A. Another particular interest for us is the development of a single planning scan for prostate patients with fiducial gold seeds. These exams would normally require two separate scans, a gradient-echo based sequence to identify the seed position and a second T2-weighted TSE for contouring the gland. The susceptibility artefact from the seed, while making them clearly visible, reduces positional accuracy, even with high bandwidths, and the requirement for two scans is less than ideal. However, we have begun looking at sequences such as turbo gradient spin-echo (TGSE) which offer the potential of combining both types of contrast into a single image (Fig. 4B).

To fully map out the geometric integrity of our system over large volumes, we have designed and built our own 3D phantom which covers 50 cm in each orientation (pictured in the magnet in Fig. 1). This test object has proved particularly useful in demonstrating the role of TimCT in cases when we have needed to exceed our 30 cm rule. By moving the patient through the bore while acquiring thin isocentric sections the distortion limit along the z-axis may be avoided altogether, thereby extending planning coverage. Figure 5 shows an example of this in a particularly difficult sarcoma case where more than 60 cm coverage was requested by the Oncologist and a total of 50 coil elements were used.

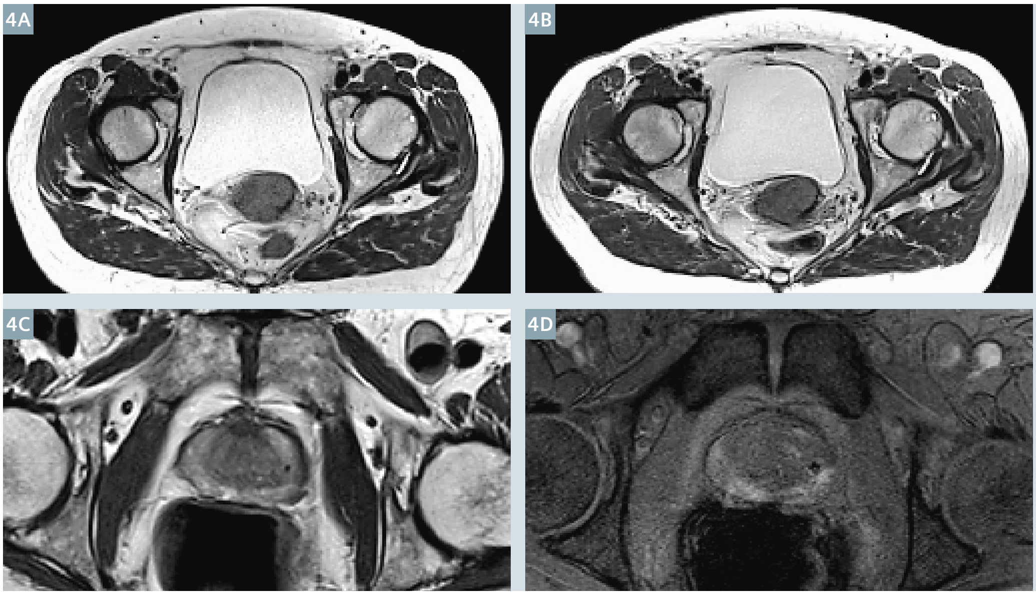


4

Developing body protocols for RT simulation; A comparison of BLADE **(4A)** versus anti-peristaltic agent **(4B)** as an effective control of organ motion artefacts. Use of the TGSE **(4C)** to provide a prostate planning scan that combines T2w contrast and gold seed visualization. **(4D)** Standard gradient-echo image used for seed localisation, which exaggerates the dimension of the marker.

## Therapy response

For most examinations we are using MRI at the commencement of treatment for its soft-tissue contrast and the improvement in planning contours. Alongside this routine work, we have begun several research studies that are using MRI to assess response over the course of treatment. These studies use both diffusion-weighted imaging (DWI) and dynamic contrast enhancement (DCE) to look at changes in tumor cellularity and vascularity respectively. In the case of diffusion, the commonly-used EPI sequence produces significant distortions and artifacts that has made its application in radiotherapy planning problematic. We have recently concluded a study that compared EPI with RESOLVE, which uses multi-segmentation in the frequency encoding direction combined with navigator self-correction, and showed improvements in ADC repeatability and geometric integrity compared to a T2-weighted gold standard [2]. Figure 6 shows a DWI example in a prostate patient acquired with $b = 800$ s/mm$^2$ together with the corresponding ADC map and we have now also adopted this sequence for rectum and cervix. As part of our DCE protocol we acquire pre-contrast sequences at 2 and 15 degree flip angles to measure the native T1 prior to using dynamically acquired TWIST images. These scans are then analysed using the two compartment model which is available with the Tissue4D software.

## Lung imaging

For our lung patients, we have developed an advanced imaging protocol providing a comprehensive assessment of anatomy, function and motion throughout their treatment (Fig. 7). For tumor contouring a T2-weighted HASTE sequence with a phase

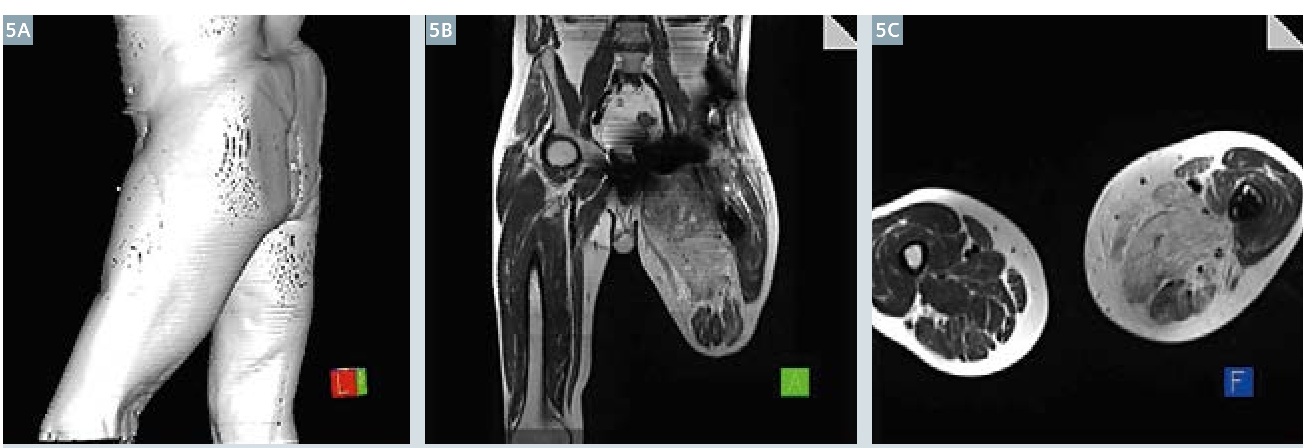


5 TimCT was used in this patient with a leg sarcoma and prosthesis *in situ* who could not straighten the effected leg. A full treatment simulation coverage of 61 cm in the head to foot direction was obtained by using the continuously moving table technique.

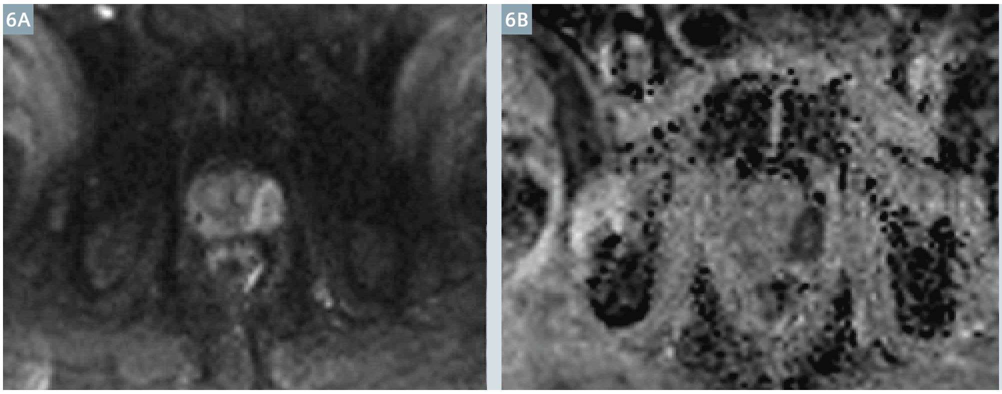


6

Diffusion-weighted imaging using the RESOLVE sequence in the prostate; **(6A)** A distortion free image with b = 800 s/mm$^2$ and **(6B)**, the resulting ADC map, both of which demonstrate an area of reduced diffusion in the left peripheral zone.

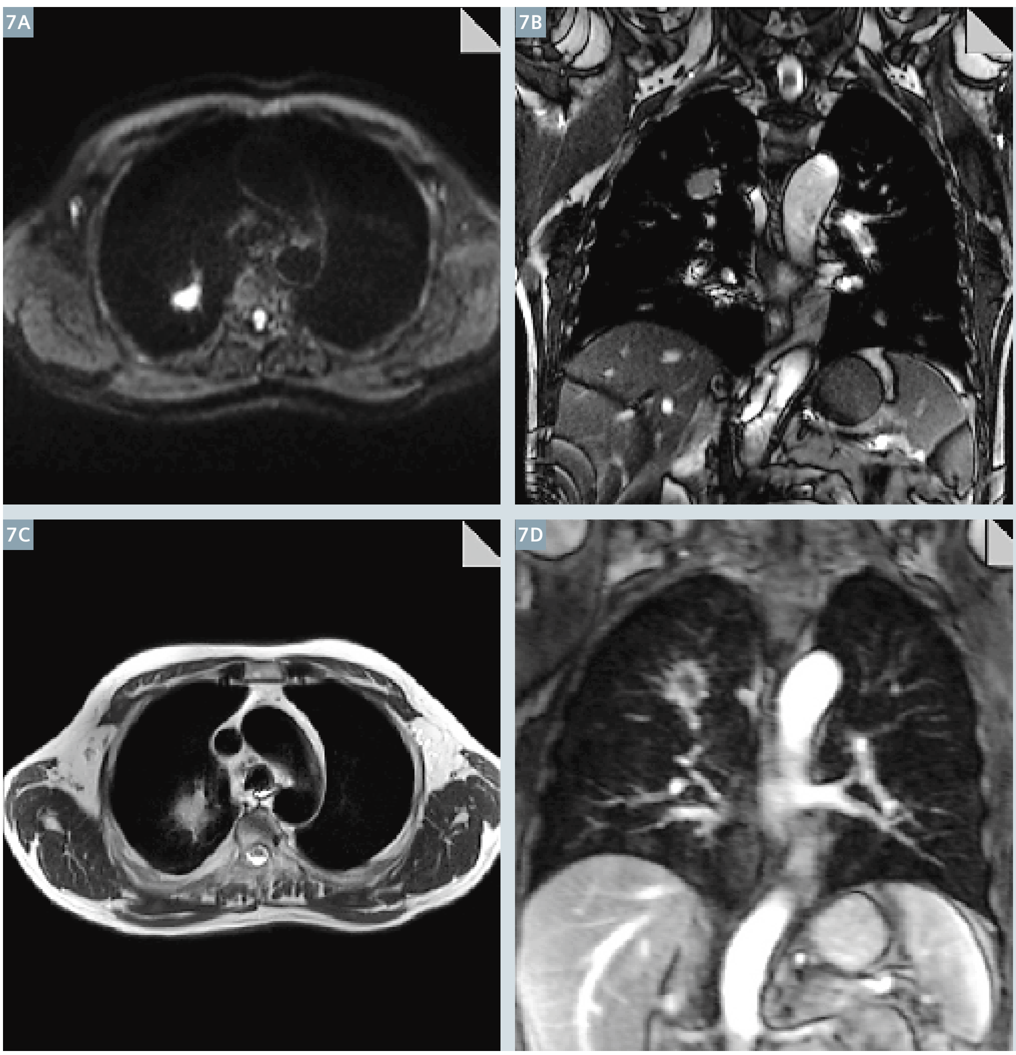


7

Example images from a lung tumor patient study; **(7A)** DWI with b = 500 s/mm$^2$ image, **(7B)** single frame from a coronal TrueFISP cine sequence acquired with cardiac shim, **(7C)** a late post-contrast enhanced TWIST image and **(7D)** axial HASTE acquired using a phase navigator.

navigator placed in the liver dome is used to provide artefact free images. We then acquire a diffusion-weighted sequence to measure ADC, and cine TrueFISP scans during free breathing to assess tumor motion. The protocol is completed with a DCE TWIST sequence which is modified to acquire a total of six separate short breath-hold windows from early first pass to 5 minutes post contrast. The incorporation of all this data is still in its infancy but we have already begun to use our own analysis to look at the tumor excursion and how it correlates with respiration.

## Conclusion

In the future, we anticipate that it will be possible to replace CT altogether in the majority of cases. In order to do this, one of the challenges will be the need to substitute CT and provide a surrogate for electron density. As part

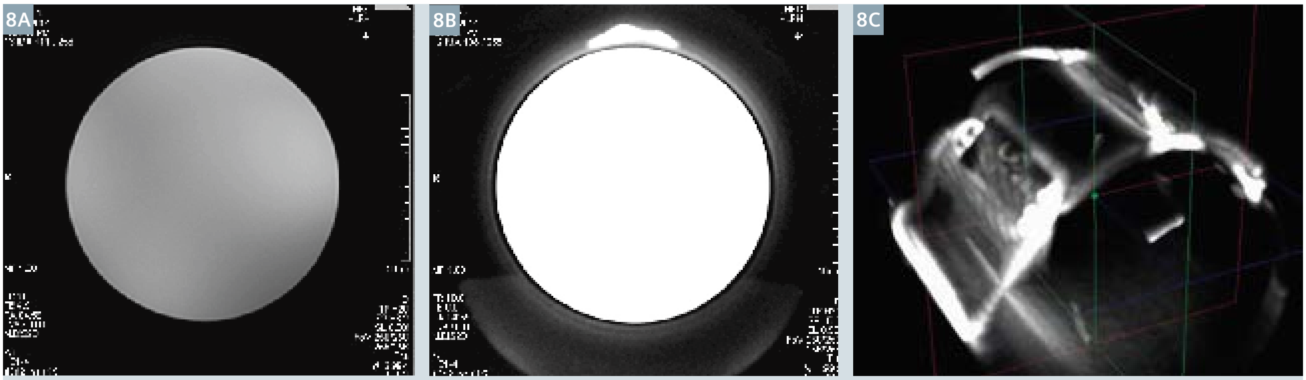


8 Examples of UTE imaging; **(8A, B)** Test object imaged at 4 ms displays signal from the fluid only but when this is repeated at 0.04 ms (40 µs) a previously invisible lump of adhesive putty placed on top and the plastic cushion underneath can also be seen. **(8C)** 3D rendering of a processed dataset which demonstrates the RF coil itself *(courtesy Jason Dowling, CSIRO)*.

of our research agreement with Siemens we are currently investigating the efficacy of ultrashort echo time (UTE) sequences to develop a strategy for MR-only planning[1]. By bringing the TE down to tens of microseconds it becomes possible to obtain signal from materials and tissues that were previously invisible (Fig. 8). These images have the potential to provide more accurate substitute CT datasets as they can map cortical bone and even the RF coil itself which will be useful on the MR-Linac.

In summary, although it is still very much early days for us, the installation of a dedicated scanner in our department has been a great success and crucial in propelling MRI into our practice. We hope that in the not-too-distant future, MR-Sim will become a fairly standard sight in many radiotherapy centres throughout Australia and indeed the rest of the world. This will certainly help to establish a standardised approach for the implementation of MRI into radiotherapy so that the full benefit of this modality can be realised.

## Acknowledgements

We would like to acknowledge the following radiotherapists who make up the MR-Sim team: Lynnette Cassapi, Ewa Juresic, Jim Yakobi & Callie Choong. Also thanks to Aitang Xing, Amy Walker (radiotherapy physicists), Mark Sidom and Dion Forstner (oncologists) and Daniel Moses (MR radiologist).

### References

1 GP Liney & MA Moerland. Magnetic resonance imaging acquisition techniques for radiotherapy planning, Sem Rad Onc in press, 2014.
2 GP Liney, T Al Harthi, E Juresic et al. Quantitative evaluation of diffusion-weighted imaging techniques for radiotherapy planning of prostate cancer. Proc ISMRM 2718: 2014.

[1] Radiotherapy Planning where MR data is the only imaging information is ongoing research. The concepts and information presented in this article are based on research and are not commercially available. Its future availability cannot be ensured.

## Contact

Associate Professor Gary Liney (UNSW)
Hon Principal Fellow, University of Wollongong
Ingham Institute for Applied Medical
Research & Radiation Oncology
Liverpool Hospital, 1 Campbell Street
Liverpool NSW 2170, Australia
Phone: +61 2 8738 9221
gary.liney@sswahs.nsw.gov.au

# Evaluation of the CIVCO Indexed Patient Position System (IPPS) MRI-Overlay for Positioning and Immobilization of Radiotherapy Patients

**Th. Koch[1]; K. Freundl[1]; M. Lenhart[2]; G. Klautke[1]; H.-J. Thiel[1]**

[1]Klinik und Praxis für Strahlentherapie und Radioonkologie, Sozialstiftung Bamberg, Germany
[2]Klinik für Diagnostische Radiologie, Interventionelle Radiologie und Neuroradiologie, Bamberg, Germany

## Abstract

The emerging development in modern radiotherapy planning (RTP) requires sophisticated imaging modalities. RTP for high precision requires exact delineation of the tumor, but this is currently the weakest link in the whole RTP process [1]. Therefore Magnetic resonance imaging (MRI) is of increasing interest in radiotherapy treatment planning because it has a superior soft tissue contrast, making it possible to define tumors and surrounding healthy organs with greater accuracy. The way to use MRI in radiotherapy can be different. The MRI datasets can be used as secondary images to support the tumor delineation. This is routinely in use in many radiotherapy departments. Two other methods of MRI guidance in the RTP process are until now only research projects, but interest in them is increasing. The first method is to use MRI data as the primary and only image dataset and the second is the application of the MRI data as reference dataset for a so-called 'MRI-guided radiotherapy in hybrid systems' (Linear Accelerator (Linac) or Cobalt RT units combined with MRI). For all cases it is essential to create the MRI datasets in the radiotherapy treatment position. For this reason the CIVCO Indexed Patient Positioning System (IPPS) MRI-Overlay was introduced and tested with our Siemens MAGNETOM Aera MRI Scanner.

## Introduction

Although computed tomography (CT) images are the current gold standard in radiotherapy planning, MRI becomes more and more interesting. Whilst CT has limitations in accuracy concerning the visualization of boundaries between tumor and surrounding healthy organs, MRI can overcome these problems by yielding superior soft tissue contrast. Currently there are three different possible strategies by which MRI can help to improve radiotherapy treatment planning:

The MRI datasets can be used as secondary images for treatment planning. These MR images can be used to delineate the tumor and the surrounding organs, whilst the CT images – the primary planning data – are necessary to calculate the 3D dose distribution. The two image datasets have to be co-registered thoroughly to ensure that the anatomy correlates (see for example [2]). The registration

1 1.5T MAGNETOM Aera with the standard cushion on the MRI couch.

2 After the removal of the standard cushion the CIVCO IPPS MRI-Overlay can be mounted.

3 The lines indicate the position for the index bars.

4 One index bar is latched to the MRI-Overlay.

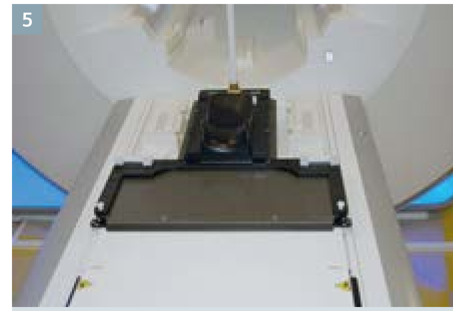

5 The mask system for head and neck fits to the index bar to avoid movement.

accuracy strongly depends on the MRI scan position. Hanvey et al. [3] and Brunt et al. [4] have shown that it is indispensable for the MRI dataset to be created in the treatment position which is primarily defined by the CT scan.

The MRI dataset can also feasibly be used as the only dataset. Because of the lack of electron density information, which is required for dosimetric calculations, bulk densities have to be applied to the MRI images. For this purpose the different anatomic regions like bone, lung, air cavities and soft tissue have to be overwritten with the physical densities. With this method it is possible to achieve dose calculation results quite similar to the calculation in the CT dataset in the head and neck region [5, 6] as well as in the pelvic region [7]. The advantage of this method is that by avoiding the CT scan you save some time and money. In this case it is necessary for the treatment position to be determined during the MRI scan, hence the MRI scanner has to be equipped with the same positioning and immobilization tools as the Linac. Further problems to overcome are the evaluation and correction of possible image distortions and the determination of accurate bulk densities.

After the RTP process there are a lot of remaining uncertainties such as set-up errors, motion of the target structures and during the treatment changes of the tumor volume and shrinking. This problem can be overcome with the so-called image-guided radiotherapy (IGRT). IGRT involves a periodical verification (weekly or more frequent) of tumor position and size with appropriate imaging systems. It is evident that IGRT is only as good as the accuracy with which the target structures can be defined. For this reason some groups try to develop hybrid systems, where a Linac or a cobalt treatment unit is combined with an MRI scanner for a so-called MR-guided radiotherapy [8-10]. Again: MR-guided radiotherapy can only be successful when the reference MRI dataset has been created in the treatment position.

In any of the above three cases, where MRI can be helpful to improve the accuracy of radiotherapy, it is strongly advised that one has a robust and reproducible patient positioning and immobilization system, mainly at the MRI scanner, which is used for MR-guided RTP. Siemens provides with the CIVCO IPPS MRI-Overlay a suitable solution. In our clinic we have introduced and tested this MRI-overlay, especially for patients with tumors in the pelvis and for brain tumors and metastasis.

## Method

Our 1.5T MAGNETOM Aera system (Siemens Healthcare, Erlangen, Germany) is located in the radiology department and can temporarily be used by the staff of the radiotherapy department. For the purpose of MR-guided RTP we have equipped the MAGNETOM Aera with the CIVCO IPPS MRI-Overlay. This overlay enables the fixation of positioning and immobilization tools necessary for radiotherapy treatments. For our purpose we have used an MR compatible mask system for head and neck cases and vacuum cushions for patients with diseases in the pelvic region both from Medical Intelligence (Elekta, Schwabmünchen, Germany). These tools can all be fixed with so-called index bars (Figs. 4, 12) at the MRI-Overlay. These index bars are custom designed for our purpose by Innovative Technologies Völp (IT-V, Innsbruck, Austria) for the MRI-Overlay and for use in the high field magnetic environment. For the correct positioning of the patients, the laser system Dorado 3 (LAP, Lüneburg, Germany) was additionally installed in the MRI room. The preliminary modifications and the patient positioning is described in the following for two cases.

The first case describes the procedure for a patient with a head tumor. The first step is the removal of the standard cushion of the MRI couch and the mounting of the MRI-Overlay (Figs. 1–3). One index bar is necessary to fix the mask system on the overlay (Figs. 4, 5) to avoid movements and rotations during the scan. Because the standard head coil set cannot be used with the mask system, two flex coils (Flex4 Large) have to be prepared (Figs. 6–8). In figure 8 one can see, that the correct head angle could be adjusted. Now the patient is placed on the overlay and in the mask system. The patient's head can be immobilized with the real and proper mask made from thermoplastic material called iCAST (Medical Intelligence, Elekta, Schwabmünchen, Germany)

6

Two flex coils (Flex4 Large) are prepared.

7

The flex coils have to be positioned partly under the mask system, because the whole head of the patient should be covered.

8

It is possible to adjust the head angle in an appropriate and reproducible position that is comfortable for the patient.

9

Now the patient is immobilized using a custom-made mask made from thermoplastic material.

10

The flex coils are closed with hook-and-loop tapes.

11

The patient is ready for the scan.

12 A custom-made vacuum cushion for the lower extremities is latched to the MRI-Overlay with two index bars.

13 A second vacuum cushion is positioned on the table to fix the arms and shoulders and keep the patient in a comfortable position.

as can be seen in figure 9. Now the flex coils can be fixed with hook-and-loop tapes and placed very tight to the patient (Figs. 10, 11). Now the MRI scan can be started.

The second case describes the preparation before the MRI scan for a patient with a tumor in the pelvic region. The first two steps are identical, the remove of the standard cushion followed by the mount of the overlay (Figs.1, 2). Then a custom-made vacuum cushion for the lower extremities is attached to the overlay with two index bars (Figs. 12, 13). For a robust position of the patients with diseases in the pelvis it is very important to keep the legs in well-defined position – not only during imaging but also throughout the

**14** Now the patient can be positioned.

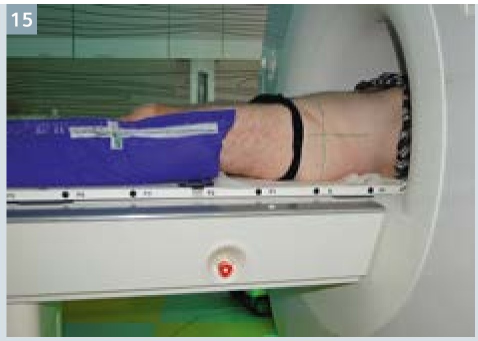

**15** The accurate position of the patient can be adjusted with the LAP laser system.

**16** A mounting-frame for the flex coil has to attached to the MRI-Overlay.

**17** The mounting-frame from a side view.

**18** The flex coil is fixed to the mounting-frame with hook-and-loop tapes.

**19** The patient is ready to start the scan.

whole treatment course, which spans over seven weeks. Any changes there can result in undesired rotations of the pelvis and in the end the tumor position and shape can also change. In figure 13 a second custom-made vacuum cushion can be seen. The only purpose of this vacuum cushion is to enable a comfortable position of the patient during scan and later during the treatment (Fig. 14). The more comfortably the patient lies on the table the more robust and reproducible is the positioning. Fortunately MAGNETOM Aera has a bore diameter of 70 cm, hence there are almost no limitations concerning patient positioning. Now the accurate position of the patient should be checked with the moveable laser-system (Fig. 15). This is necessary to avoid rotations of the pelvis around the patients longitudinal and lateral axis. For the fixation of the flex-coil for the pelvic region a mounting-frame has to be attached to the overlay (Figs. 16, 17). This can be done with hook-and-loop tapes (Fig. 18). Now the patient set-up is completed and the MRI scan can be started (Fig. 19).

## Results

Two examples are shown in the following pictures. In Fig. 20 you can see a brain tumor in two corresponding slices. The left picture shows the CT-slice and the right picture shows the corresponding MRI slice obtained with a T1-weighted sequence with contrast agent. It is clear to see that tumor boundary is much more pronounced in the MRI image. Figure 21 shows the same slices with structures created by the radiotherapists. It is also helpful to create some control structures, such as brain and ventricles, to check the accuracy of the registration. Figures 22 and 23 give an example of a patient with prostate cancer. In this case the MRI images on the right

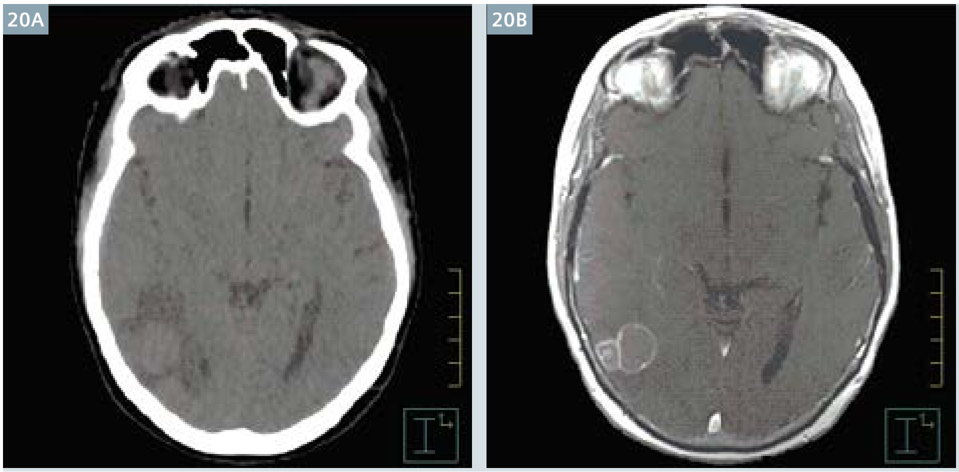


**20**

Two corresponding slices of a brain scan: **(20A)** CT slice and **(20B)** MRI slice obtained using a T1-weighted sequence with contrast agent.

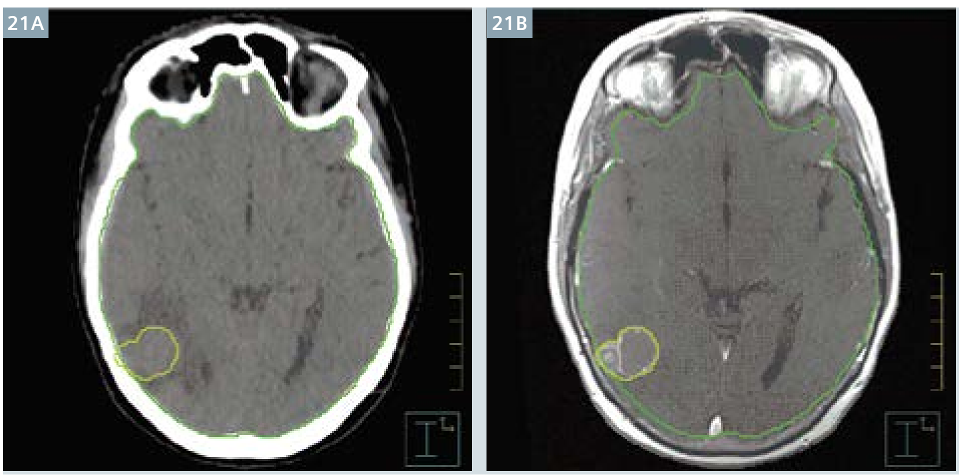


**21**

The same slices as in figure 20, but now with delineated tumor and help structures.

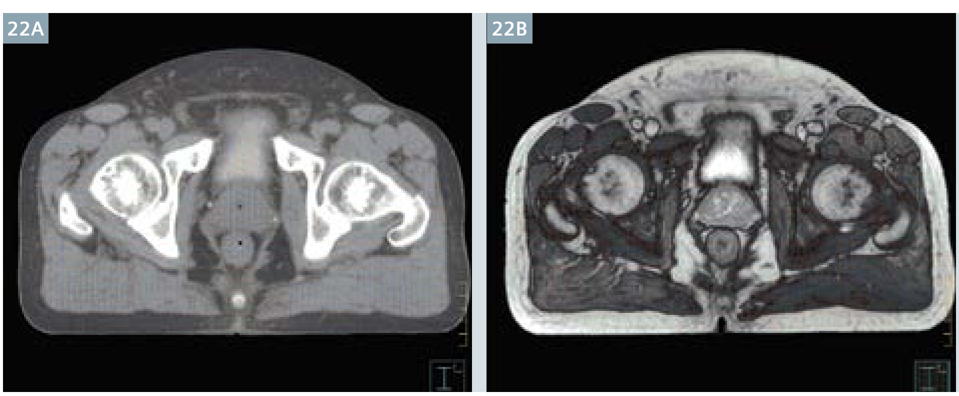


**22**

Two corresponding slices in the pelvic region of a patient with a prostate cancer: **(22A)** CT slice and **(22B)** MRI slice obtained with a T2-weighted TrueFISP sequence.

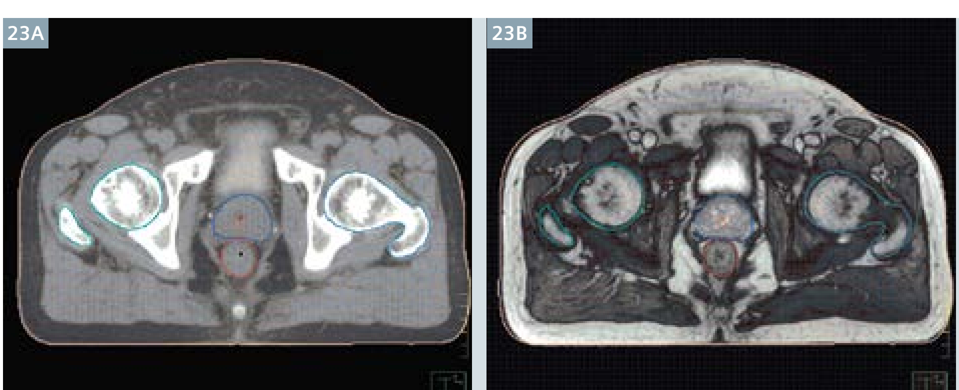


**23**

The important structures rectum and prostate as defined in the MRI slice are shown. The accuracy of the registration can be tested with the coincidence of help structures – like the femoral heads in this case – in both datasets.

are acquired using a T2-weighted TrueFISP sequence. The boundary of the prostate and the differentiation between prostate and rectum is much more easier to define in the MRI images. The control structures in this case are the femoral heads. For the head scans we normally use 3 sequences, a T1w SE with contrast agent, a T2w TSE and a FLAIR sequence. For the pelvis scans we normally use a T2w SPACE, a T2w TrueFISP and a T2w TSE sequence. The coordinate system should be the same for all sequences, that means same slices and same field-of-view. Hence one can use the same registration parameters for all sequences.

## Conclusion and outlook

We can now look back over a period of two years working with the CIVKO IPPS MRI-Overlay. Our experience is very promising. The modifications on the table of the MRI scanner are very easy and can be executed and finished in only a couple of minutes. The procedure is well accepted by the radiologic technologists. To date, we have scanned more than 100 radiotherapy patients, mainly with diseases in the pelvis (rectum and prostate cancer) and in the head (brain tumors and metastasis). So far we have only used MRI dataset as a secondary image dataset. The co-registration with the CT datasets is now much easier because we have nearly identical transversal slices in both image datasets.

As a conclusion we can say that we are very happy with the options we have to create MRI scans in the treatment positions. It has been demonstrated that the MRI dataset is now much more helpful in the radiotherapy planning process. We should mention the need for a quality assurance program to take possible image distortions into consideration. Our next step is to install such a program, which involves the testing of suitable phantoms. A further step will be to assess whether we can use MRI datasets alone for RTP.


### References

1. Njeh C. F. Tumor delineation: the weakest link in the search for accuracy in radiotherapy. J. Med. Phys. 2008 Oct-Dec; 33(4): 136-140.
2. Dean C.J. et al. An evaluation of four CT-MRI co-registration techniques for radiotherapy treatment planning of prone rectal cancer patients. Br. J. Radiol. 2012 Jan; 85: 61-68.
3. Hanvey S. et al. The influence of MRI scan position on image registration accuracy, target delineation and calculated dose in prostatic radiotherapy. Br. J. Radiol. 2012 Dec; 85: 1256-1262.
4. Brunt J.N.H. Computed Tomography – Magnetic Resonance Imaging Registration in Radiotherapy Treatment Planning. Clin. Oncol. 2010 Oct; 22: 688-697.
5. Beavis A.W. et al. Radiotherapy treatment planning of brain tumours using MRI alone. Br. J. Radiol. 1998 May; 71: 544-548.
6. Prabhakar R. et al. Feasibility of using MRI alone for Radiation Treatment Planning in Brain Tumors. Jpn. J. Clin. Oncol. 2007 Jul; 37(6): 405-411.
7. Lambert J. et al. MRI-guided prostate radiation therapy planning: Investigation of dosimetric accuracy of MRI-based dose planning. Radiother. Oncol. 2011 Mar 98: 330-334.
8. Raymakers B.W. et al. Integrating a 1.5 T MRI scanner with a 6 MV accelerator: proof of concept. Phys. Med. Biol. 2009 May; 54: 229-237.
9. Hu Y. et al. Initial Experience with the ViewRay System – Quality Assurance Testing of the Imaging Component. Med. Phys. 2012 Jun; 39:4013.
10. ViewRay. Available at: http://www.viewray.com


## Contact


Thomas Koch, Ph.D.
Sozialstiftung Bamberg – Medizinisches Versorgungszentrum am Bruderwald
Praxis für Radioonkologie und Strahlentherapie
Head Medical Physics
Buger Straße 80
96049 Bamberg
Germany
Phone: +49 951 503 12931
thomas.koch@sozialstiftung-bamberg.de

# RT Dot Engine

**Gregor Thörmer, Ph.D.; Martin Requardt, Ph.D.**

Siemens Healthcare, Magnetic Resonance Imaging, Erlangen, Germany

## Background

Magnetic resonance imaging (MRI) is based on different *pulse sequences*, a combination of radiofrequency pulses and gradients that are switched on and off according to a specific scheme. The strength, duration, and spacing of these 'building blocks' are defined by imaging *parameters*. This allows the depiction of tissue in various ways, e.g. for the visualization of vessels, fat or edema, and with different spatial and temporal resolution, depending on the concrete clinical question. An imaging *protocol* allows predefined or customized parameter sets to be saved and retrieved [1].

Standard MR imaging protocols for diagnostic purposes are typically not optimized to meet the requirements of radiation therapy (RT), but can be adjusted for high spatial integrity, isotropic voxels and reduced susceptibility to motion artifacts via the underlying imaging parameters. To do so, however, the user had to be familiar with the complex system of parameters and their mutual interference up to now [2].

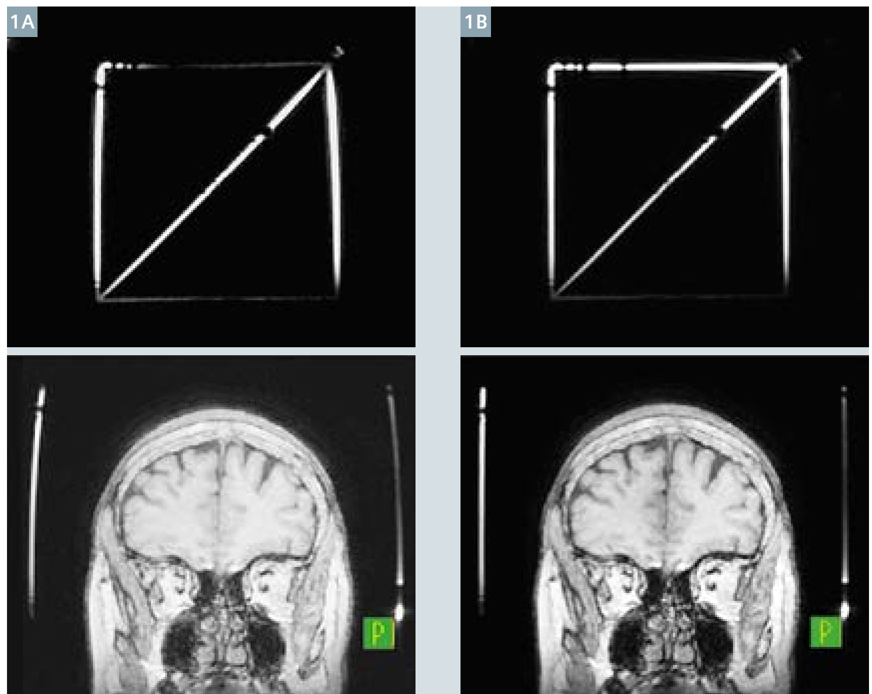


1 Left column **(1A)** shows uncorrected MR images with distortions due to gradient non-linearity. In the right column **(1B)**, these distortions are automatically corrected with 3D distortion.

## RT Dot Engine

With the RT Dot[1] Engine, a comprehensive package became available addressing specifically the requirements of MR imaging for radiation therapy. The imaging protocols it provides have been developed in collaboration with RT departments experienced in using MR, in particular the group of Prof. James Balter (Michigan University, Ann Arbour, USA). Features like automatic axial image reconstruction and 'one click' integration of external laser bridges are easily accessible. All protocols in the RT Dot Engine were carefully optimized to improve spatial integrity, e.g. via high bandwidths [2] and automatic 3D distortion correction (Fig. 1). In the "Dot mode", only a limited set of routine geometry parameters is shown to the user (Fig. 2), while the "Detail mode" provides full access to imaging parameters. The product features different predefined strategies for brain and head & neck imaging and a protocol to perform external Laser QA (Fig. 3). Using this technology, Radiation Oncology staff can perform MR exams in a reliable and reproducible way. Furthermore, pictograms and hints that exemplary show how to plan an exam can be used to guide less MR-experienced users troughout the workflow. More advanced customers can use the dedicated RT Dot AddIns to build their own RT Dot Engines for other body regions. To support this, Siemens has a team of MR application specialists specifically trained for RT.

## One click integration of external lasers

After patient preparation and positioning with MR compatible immobilization accessories, an external laser bridge (DORADOnova, LAP, Germany) can be used to exactly define the target position on the patient's body. In the past, the technologist had to perform this step with the built-in laser crosshair of the MRI system again; a handicap of the workflow and a source of inaccuracy. Now, a Dot AddIn takes care with 'one click' ("Laseroffset-Scan", see Fig. 3) that the position defined with the external laser beam directly goes to the center of the magnet where imaging conditions are optimal. One enabler of this technology is the ±0.5 mm positioning accuracy of the Tim Table[2].

2 User interface shows the predefined scan strategy for a brain exam with the RT Dot Engine. The queue with RT protocols is displayed in the lower half to the left. In "Dot mode" a limited set of geometry parameters is displayed on the right side to adapt scanning to patient's anatomy. By clicking the magnifying glass symbol in the lower right corner you can access and define all imaging parameters on expert level.

## Fine structured scanning and spatial integrity

Imaging in the treatment position with thermoplastic masks and other equipment requires the use of flexible surface coils. Two such coils wrapped around the patient's head form an '8-channel head coil' providing 17% increase in signal-to-noise-ratio (SNR) compared to a setup with two loop coils positioned left and right of the skull. Nonetheless, the received SNR is still approximately 25% higher with a dedicated 20-channel head & neck coil.

To address this challenge, the RT Dot Engine allows acquisition of two interleaving datasets with an overlap ('negative distance factors') of the neighboring slices. To give an example: 3 mm slice thickness and a negative distance factor of 50% corresponds to an effective interslice distance of only 1.5 mm. This technique of fine structured 2D scanning not only improves the SNR of reconstructed images, it also supports 3D reformatting capabilities (Fig. 4)

## 3D imaging and automatic axial image reconstruction

A majority of imaging protocols in the RT Dot Engine is based on 3D sequences. 3D images inherently provide superior SNR compared to 2D imaging, allow for isotropic voxel size and can be reformatted in any desired orientation. From the point of MR physics it is sometimes beneficial to acquire these datasets with non-axial slice orientation. For some therapy planning systems, however, axial image orientation is mandatory.

3 Scan strategies within the RT Dot Engine for MAGNETOM Skyra [204x48].

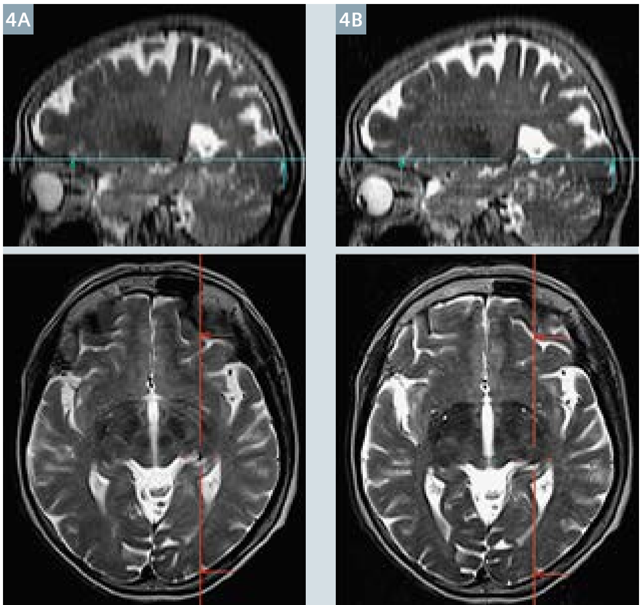


4 Comparison of a standard axial 2D TSE scan with no gap between the slices **(4A)** and a fine structured 2D TSE volume scan **(4B)**. These images provide both better SNR and good delineation of anatomical structures along the slice axis. The technique is applicable to every 2D sequence protocol.

5 Screenshot of multiplanar reconstruction (MPR) planning AddIn. Assigned image data sets (here: 4 t1_spc_sag_reformat_tra and 5 t2_spc_flair_reformat_tra) are automatically reconstructed according to the defined parameters.


6 Left: Coordinate Frame G inside a Tx/Rx (transmit/receive) head coil. By clicking “measure” the B1 rms value for a protocol is calculated. In the example shown here, the flip angle, which correlates with the power of the applied refocusing RF pulses was reduced from 180° to 150° resulting in a respective decrease of the applied average RF power.

In the RT Dot Engine an AddIn ensures that axial images are automatically reconstructed in a predefined way which then can be sent to the planning system (Fig. 5). If a user always wants to have 1.5, 3 and 6 mm axial slices, for example, this can be defined via a respective preset.

## B1 rms calculation

Some radiation therapy scenarios involve the use of special equipment, like dedicated stereotactic head-frames to fixate the patient’s skull. For some devices special regulations exist, i.e. to operate these devices with protocols under restricted RF-deposition in order to reduce the risk of heating during imaging[3]. The functionality “B1 rms” (Root mean square of the B1 field) enables easy access to SAR (specific absorption rate) deposition with a specific imaging protocol (Fig. 6). Before starting the actual measurement, the user can verify if certain safety conditions are fulfilled and change imaging parameters if necessary.

### References

1 Rumpel H, et al. How Modules of Imaging Sequences Fit Together: An Overview of Recent Advances in MR Imaging. MAGNETOM Flash #60 (5/2014) p86-92.
2 Graessner J. Bandwidth in MRI? MAGNETOM Flash #52 (2/2013) p122-127. http://www.healthcare.siemens.com/magnetic-resonance-imaging/magnetom-world/clinical-corner/application-tips/bandwidth-mri

## Contact

Gregor Thörmer, Ph.D.
Global Segment Manager Men’s and Women’s Health
Siemens Healthcare
Karl-Schall-Str. 6
91052 Erlangen
Germany
gregor.thoermer@siemens.com

[1] Dot (Day optimizing throughput) includes different features like Dot AddIns to assist the user, standardize procedures and automate recurrent workflow steps.

[2] Specifications MAGNETOM Aera and MAGNETOM Skyra. Datasheet.

[3] Specifications and terms of use are defined and provided by the manufacturer of the equipment.

# Anatomical and Functional MRI for Radiotherapy Planning of Head and Neck Cancers

Maria A. Schmidt, Ph.D.; Rafal Panek, Ph.D.; Erica Scurr, DCR(R), MSc; Angela Riddell, MD FRCS FRCR; Kate Newbold, MD MRCP FRCR; Dow-Mu Koh, MD MRCP FRCR; Martin O. Leach, Ph.D. FMedSci

Cancer Imaging Centre, Royal Marsden NHS Foundation Trust and Institute of Cancer Research, Sutton, UK

## Introduction

Head and Neck cancers are relatively common: squamous cell carcinoma of the head and neck (SCCHN) has a worldwide incidence of approximately 500,000 cases per annum [1]. Treatment is a combination of surgery, chemotherapy and radiotherapy (RT), devised to maximize the probability of eradicating the disease while retaining organ function [2-5]. Recent technical advances in RT include high-precision conformal techniques such as intensity-modulated RT (IMRT) and volumetric intensity modulated arc therapy (VMAT), which enable dose escalation to lesions without exceeding recommended exposure levels for organs at risk (OAR). However, these techniques require accurate anatomical information to contribute towards improving disease control.

High-resolution Magnetic Resonance Imaging (MRI) has increasingly been used to plan Head and Neck RT [6-10]. MRI and CT images are registered, combining the advantageous soft tissue contrast of MRI examinations and the required CT-based electron density. However, MR images are often distorted due to magnetic field inhomogeneity and non-uniform gradients [11-13], and the use of CT-MR fusion requires geometrically accurate MRI datasets. This article describes the equipment, protocols and techniques used in Head and Neck MRI at the Royal Marsden NHS Foundation Trust to ensure that the MRI examinations undertaken for RT planning purposes achieve the required geometric accuracy.


1 Receiver coil arrangement used at the Royal Marsden NHS Foundation Trust to perform Head and Neck MRI for RT planning. A standard MR-compatible baseboard is employed, enabling the use of a thermoplastic mask. The large flex-coil is positioned above the neck and used in conjunction with elements of the spine array.

## High resolution anatomical imaging in the radiotherapy planning position

At the Royal Marsden NHS Foundation Trust clinical Head and Neck MRI examinations for RT planning are undertaken at 1.5T in the 70 cm bore MAGNETOM Aera (Siemens Healthcare, Erlangen, Germany). Patients are scanned in the RT position using an appropriate head rest and thermoplastic shell immobilisation attached to an MR-compatible headboard, modified to remain accurately positioned on the Aera patient couch. In addition to the elements of the posterior spine coil selected at the level of the lesion, a large flex-coil is also placed anteriorly, in line with the tumor, employing a custom-built plastic device to keep the coil curved, following the neck anatomy. This arrangement achieves a high signal-to-noise ratio, allows effective use of parallel imaging and keeps patient comfort in the RT planning position (Fig. 1).

The MRI protocol covers the primary tumor and neck lymph nodes with approximately isotropic T1-weighted sagittal 3D acquisition (TE 1.8 ms, TR 880 ms, 160 x 1 mm slices, 250 mm x 250 mm FOV, 256 x 256 image matrix). Images are acquired post contrast-agent injection (single dose). This dataset is subsequently registered with the RT planning CT examination, and for this reason its geometric integrity is checked periodically with a large linear test object, previously described [14], consisting of sets of straight tubes in three orthogonal directions. Figure 2 shows images of the test object without and with post processing to correct image distortion. The 3D distortion correction built into the scanner software is essential for RT planning, and always used. The maximum displacement found within the volume encompassed by head and neck examinations is less than 1 mm. In addition, the imaging protocol employs a 500 Hz/pixel band-width, ensuring chemical shift related displacements in the readout direction remain under 0.5 mm.

Having characterized the geometric integrity of the protocol employed, it is also essential to characterize any further distortion associated with the distribution of magnetic susceptibility values within the subjects. In Head and Neck a large number of air-tissue interfaces in the vicinity of the tumors gives rise to localized magnetic field inhomogeneity, detrimental to the geometric integrity of the images. For this purpose, the field inhomogeneity in this region was estimated in five Head and Neck subjects. Transaxial gradient-echo images were acquired with fat and water in phase (TE values 4.76 and 9.53 ms), and the phase images were subtracted. The local field inhomogeneity was measured after phase unwrapping. Displace-ments associated with the airways were mostly under 0.5 mm with this sequence. Displacements only reach 1 mm in the vicinity of dental implants, and only very few pixels are affected.

## Functional imaging

In addition to the clinical service pro-viding anatomical images for RT plan-ning, functional MRI is also employed to characterize lesions pre and post treatment and to investigate predic-tion of treatment response both at 1.5T (MAGNETOM Aera) and 3T (MAGNETOM Skyra). In RT planning, the ultimate aim of functional imag-ing techniques is to identify radio-resistant disease and thus provide a biological target volume for dose boosting. Geometric accuracy is therefore essential to allow correct registration of functional MR images with anatomical MRI and CT datasets. In Head and Neck cancers, both diffu-sion-weighted imaging (DWI) and Dynamic Contrast-Enhanced (DCE) MRI have been explored [15-21].

**Diffusion-weighted imaging with readout segmentation of long variable echo-trains (RESOLVE):** EPI-based DWI is sensitive to the mobility of water molecules and to their environment. In cancer, cell proliferation is often associated with an increase in cell density and in extracellular space tortuosity. This leads to lower values of the Apparent Diffusion Coefficient (ADC), com-pared to healthy tissues [22-23]. ADC values have thus been used for tumor detection, prediction and assessment of treatment response.

EPI in regions adjacent to air-tissue interfaces is known to suffer from poor geometric integrity [24]. Because this affects Head and Neck studies, strategies to reduce the echo-train length were sought. In addition to parallel imaging, the RESOLVE technique was also employed to acquire multi-shot DWI using a navigator signal to enable accurate multi-echo combinations. In Head and Neck studies, DWI with RESOLVE was employed, covering the volume of interest to identify restricted diffusion within primary lesions and affected lymph nodes.

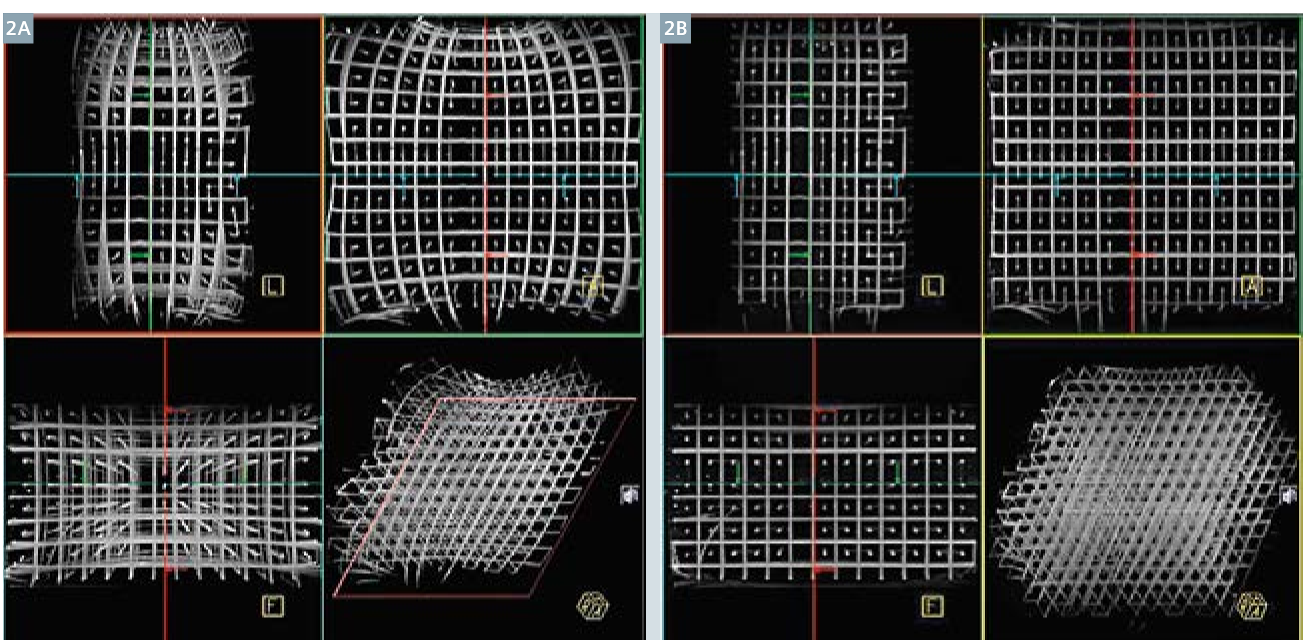


2 Images of the Linear Test Object (described by Doran et al. [14]) acquired using a 3D T1-weighted sequence with bandwidth 500 Hz/pixel, without distortion correction **(2A)** and with 3D distortion correction **(2B)**. Each picture shows three maximum intensity projections (sagittal, coronal and transaxial) and a 3D view of the test object.


**3** A comparison of conventional single shot DWI **(3A)** and RESOLVE DWI **(3B)** in a head examination. The ADC calculated with the RESOLVE DWI **(3C)** retains the geometric integrity. Standard DWI parameters: TE 98 ms, TR 7000 ms, receiver bandwidth 1040 Hz/pixel, matrix 192 x 192, FOV 230 mm x 230 mm, 3 averages, slice thickness 4 mm. RESOLVE DWI parameters: TE 58 ms, TR 5700 ms, receiver bandwidth 950 Hz/pixel, matrix 128 x 128, FOV 240 mm x 240 mm, slice thickness 4 mm.

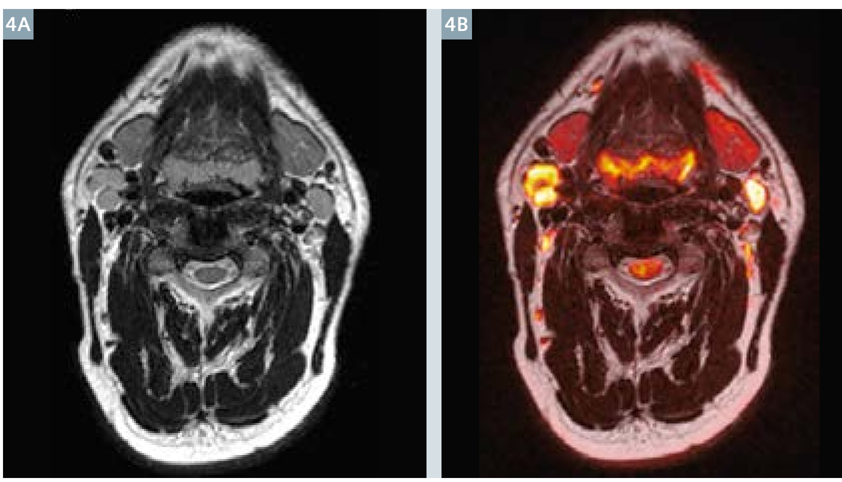


**4** Head and Neck T2-weighted image **(4A)** with co-registered RESOLVE diffusion-weighted image **(4B)**. Restricted diffusion (high intensity) can be observed in nodes, spinal cord, tonsils and submandibular glands with no apparent geometrical distortion.

Figure 3 compares DWI acquired without and with the RESOLVE technique for a Head subject, in a slice comprising air spaces. The clear improvement in geometric integrity achieved with RESOLVE DWI allows the registration of anatomical and functional images, thus allowing the use of DWI in RT planning for Head and Neck cancers (Fig. 4).

**Dynamic contrast-enhanced MRI with CAIPIRINHA-VIBE and TWIST view-sharing*:**
In dynamic contrast-enhanced (DCE)-MRI a series of 3D T1-weighted images is acquired to monitor contrast-agent uptake following an intravenous injection of contrast-agent. Using reference images, this technique can be quantitative and provide a dynamic calculation of T1 for each voxel. This enables pharmacokinetic modelling, providing information on tumor microcirculation, vascularity, blood volume and vessel permeability [25, 26]. This quantitative approach to DCE requires high temporal resolution to maintain accuracy. However, this conflicts with the need for high spatial resolution in RT planning applications.

The combination of flex-coil and spine coil elements has been used for DCE employing TWIST view-sharing and CAIPIRINHA reconstruction to produce high resolution images (voxel size 2 mm isotropic x 44 slices, CAIPIRINHA parameters: 2x2) with 2.5 s temporal resolution (TWIST parameters: A = 33% B = 33%). An example of TWIST/CAIPIRINHA DCE with a generous superior/inferior coverage to include both primary site and local involved lymph nodes is shown in figure 5. Isotropic voxels allow for a good 3D delineation of a biological target volume. In addition, Dixon reconstruction of fat and water images also provides information on fat content within the imaged volume, which might be important in the context of tumor response to treatment. Figure 6 shows T1-weighted water-Dixon signal change after Gd injection for a given representative slice containing a primary tumour. Last frame shows K**trans** map within the region of interest.

* The product is still under development and not commercially available yet. Its future availability cannot be ensured.

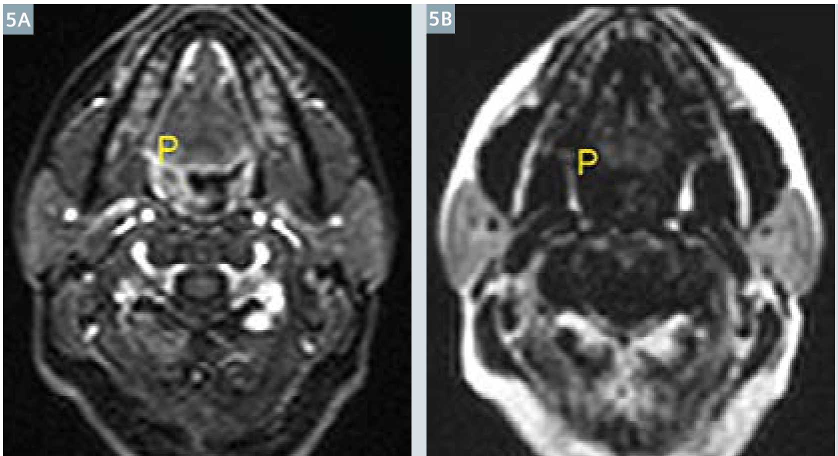


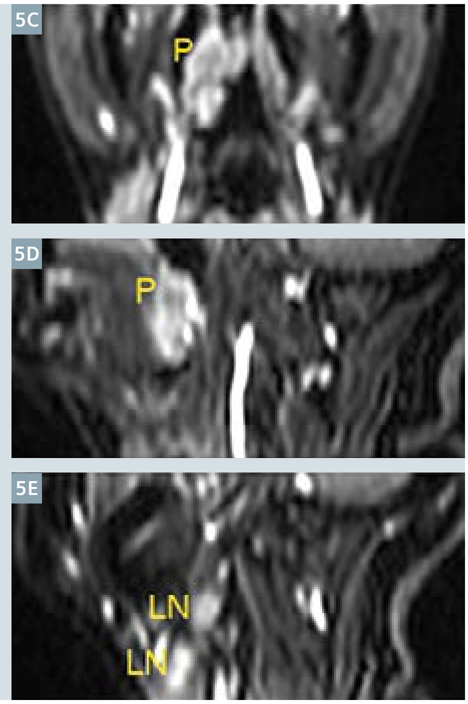


**5** Post-contrast water **(5A)** and fat **(5B)** Dixon images of patient with squamous cell cancer of the head and neck. Isotropic voxels allow for a good assessment of primary (P) and nodal (LN) tumour site (**5C–E**; coronal and sagittal image reconstruction). DCE protocol: Flip angle 4/24 degrees, TR 7.2 ms, $TE_1$ 2.4 ms, $TE_2$ 4.8 ms, 2 mm isotropic resolution in 44 slices, temporal resolution 2.5 s (TWIST: A = 33%, B = 33%, CAIPI: 2 x 2).

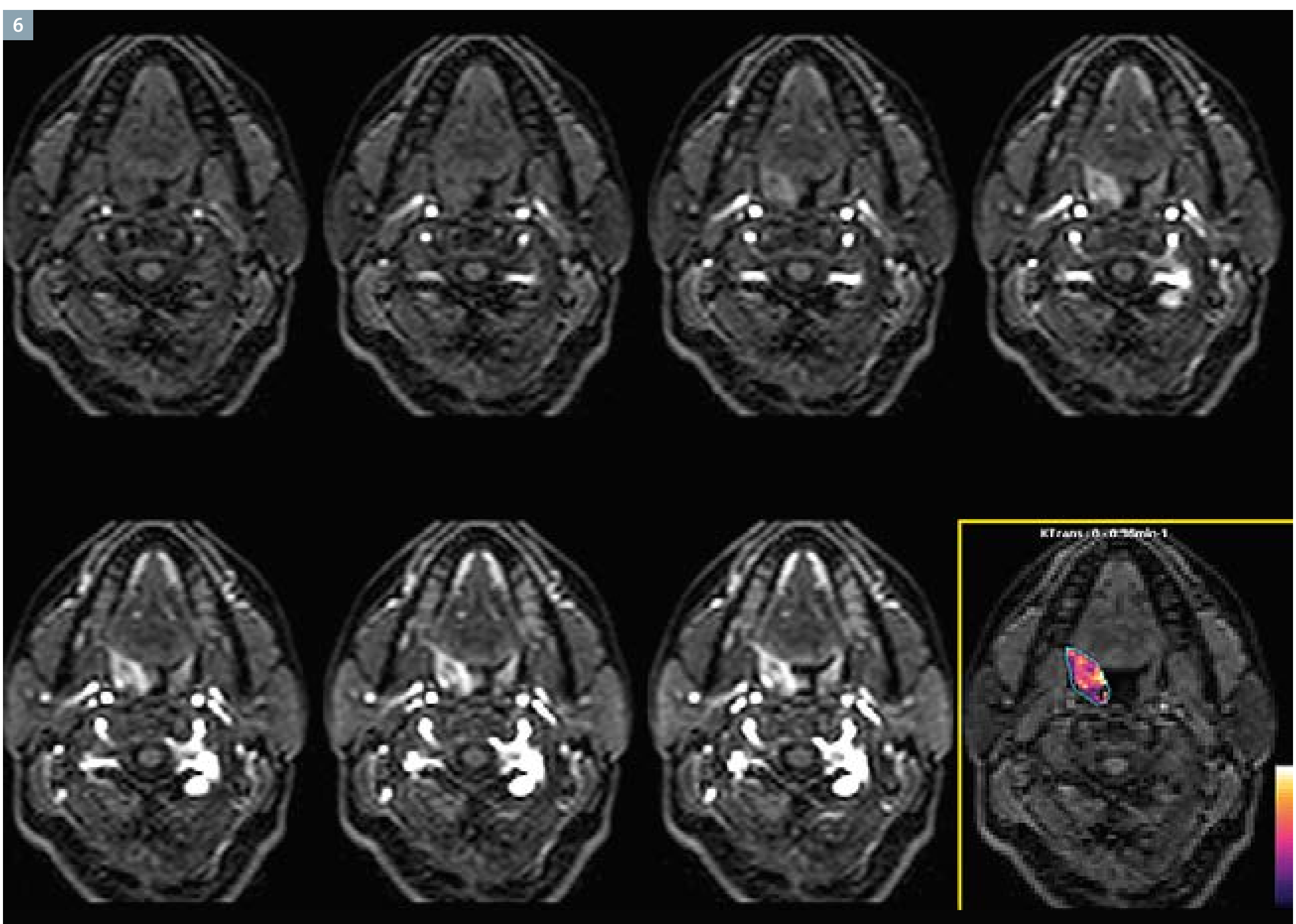


**6** T1-weighted Dixon/water signal change after contrast agent injection, showing progressive enhancement and washout of Head and Neck cancer lesion. Last frame shows K**trans** for a region of interest over a primary tumor site.

## Conclusion

Geometrically accurate anatomical and functional imaging for RT planning of Head and Neck cancers were acquired in the RT planning position in standard clinical scanners; this service was developed to meet the clinical and research needs of the users, using custom built coil positioning devices and test objects.

## Acknowledgments

The authors wish to thank D. Nickel, R. Kroeker and P. Ravell (Siemens Healthcare) for the provision of the works-in-progress package WIP771 (VIBE with View Sharing TWIST). The authors acknowledge the support of CRUK and EPSRC to the Cancer Imaging Centre at ICR and RMH in association with MRC & Department of Health C1060/A10334, C1060/A16464 and NHS funding to the NIHR Biomedicine Research Centre and the Clinical Research Facility in Imaging. This work was also supported in part by Cancer Research UK Programme Grants C46/A10588 and C7224/A13407. MOL is an NIHR Senior Investigator.



### Contact

Dr. Maria A. Schmidt
MRI Unit
Royal Marsden NHS
Foundation Trust
Downs Rd
Sutton SM2 5PT
UK
Phone: +44 (0)20 8661 3353
maria.schmidt@icr.ac.uk

### References

1 Parkin DM, Bray F, Ferlay J, Pisani P. Estimating the world cancer burden: Globocan 2000. International Journal of Cancer. 2001;94(2):153–6.
2 Bentzen SM, Trotti A. Evaluation of early and late toxicities in chemoradiation trials. J Clin Oncol 2007; 25:4096-4103.
3 Harrington KJ, et al. Interactions between ionising radiation and drugs in head and neck cancer: how can we maximise the therapeutic index? Curr Opin. Investig Drugs 2002; 3: 807-11.
4 Lefebvre JL, et al. Larynx preservation clinical trial design: key issues and recommendations - a consensus panel summary. Int J Radiat Oncol Bioi Phys. 2009; 73: 1293-303.
5 Kazi R, et al. Electroglottographic comparison of voice outcomes in patients with advanced laryngopharyngeal cancer treated by chemoradiotherapy or total laryngectomy. Int J Radiat Oncol Bioi Phys. 2008; 70: 344-52.
6 Ahmed M, Schmidt M, Sohaib A, Kong C, Burke K, Richardson C, Usher M, Brennan S, Riddell A, Davies M, Newbold K, Harrington KJ & Nutting CM. The value of magnetic resonance imaging in target volume delineation of base of tongue tumours – a study using flexible surface coils. Radiother Oncol 2010; 94, 161-7.
7 Bhide SA, Ahmed M, Barbachano Y, Newbold K, Harrington KJ & Nutting CM. Sequential induction chemotherapy followed by radical chemo-radiation in the treatment of locoregionally advanced head-and-neck cancer. Br J Cancer 2008; 99, 57-62.
8 Gregoire V et al. Radiotherapy for head and neck tumours in 2012 and beyond: conformal, tailored, and adaptive? Lancet Oncol. 2012; 13(7), pp.e292-300.
9 Nuyts S. Defining the target for radiotherapy of head and neck cancer. Cancer Imaging.2007;7(Special Issue A):S50–S55.
10 Newbold K, Partridge M, Cook G, Sohaib SA, Charles-Edwards E, Rhys-Evans P, et al. Advanced imaging applied to radiotherapy planning in head and neck cancer: a clinical review. Br J Radiol. 2006 Jul 1;79(943):554–61.
11 Wang D & Doddrell DM. Geometric distortion in structural magnetic resonance imaging. Current Medical Imaging Reviews 2005; 1: 49-60.
12 Wang H, Balter J & Cao Y. Patient-induced susceptibility effect on geometric distortion of clinical brain MRI for radiation treatment planning on a 3T scanner. Phys Med Biol. 2013; 58: 465-77.
13 Reinsberg SA, Doran SJ, Charles-Edwards EM & Leach MO. A complete distortion correction for MR images: II. Rectification of static-field inhomogeneities by similarity-based profile mapping. Phys Med Biol 2005; 50: 2651-61.
14 Doran SJ, Charles-Edwards L, Reinsberg SA & Leach MO. A complete distortion correction for MR images: I. Gradient warp correction. Phys Med Biol. 2005; 50: 1343-61.
15 Thoeny HC, de Keyzer F & King AD. Diffusion-weighted MR imaging in the head and neck. Radiology, 2012; 263(1): pp.19-32.
16 Vandecaveye, V. et al. Evaluation of the larynx for tumour recurrence by diffusion weighted MRI after radiotherapy: initial experience in four cases. The British Journal of Radiology 2006; 79: 681-687.
17 Sumi M, Sakihama N, Sumi T, Morikawa M, Uetani M, Kabasawa H, et al. Discrimination of metastatic cervical lymph nodes with diffusion-weighted MR imaging in patients with head and neck cancer. AJNR Am J Neuroradiol 2003; 24(8):1627-34.
18 Powell C, Schmidt M, Borri M, Koh DM, Partridge M, Riddell A, Cook G, Bhide S A, Nutting CM, Harrington KJ & Newbold KL. Changes in functional imaging parameters following induction chemotherapy have important implications for individualised patient-based treatment regimens for advanced head and neck cancer. Radiother Oncol. 2013; 106, 112-
19 Quon H, Brizel DM. Predictive and prognostic role of functional imaging of head and neck squamous cell carcinomas. Semin Radiat Oncol. 2012 Jul; 22(3):220–32.
20 Wang P, Popovtzer A, Eisbruch A, Cao Y. An approach to identify, from DCE MRI, significant subvolumes of tumours related to outcomes in advanced head-and-neck cancer. Medical Physics. 2012; 39(8):5277–85.
21 Srinivasan A, Mohan S & Mukherji SK. Biological imaging of head and neck cancer: the present and the future. AJNR Am J Neuroradiol. 2012; 33(4), pp. 1-9.
22 Padhani et al. Diffusion-Weighted Magnetic Resonance Imaging as a Cancer Biomarker: Consensus and Recommendations, Neoplasia 2009; 11(2):102-125.
23 Galbán CJ et al. The parametric response map is an imaging biomarker for early cancer treatment outcome. Nature medicine, 2009;15(5): pp.572-6.
24 Jezzard P. Correction of geometric distortion in fMRI data. Neuroimage 2012; 62: 648-51.
25 Walker-Samuel S, Leach MO, Collins DJ. Evaluation of response to treatment using DCE-MRI: the relationship between initial area under the gadolinium curve (IAUGC) and quantitative pharmacokinetic analysis. Phys Med Biol. 2006 Jul 21; 51(14):3593–602.
26 O'Connor J P B, Jackson A , Parker G J M and Jayson G C. DCE-MRI biomarkers in the clinical evaluation of antiangiogenic and vascular disrupting agents. British Journal of Cancer 2007; 96: 189–195. doi:10.1038/sj.bjc.6603515.

# Clinical Application of Diffusion Tensor Imaging in Radiation Planning for Brain Tumors

S. Rogers[1]; S. Bodis[1]; G. Lutters[1]; L. Remonda[2]; J Berberat[1, 2]

[1]Radiation Oncology, Canton Hospital, Aarau, Switzerland
[2]Neuro-radiology, Canton Hospital, Aarau, Switzerland

Malignant brain tumors (glioma WHO grade III-IV) are notoriously difficult to treat despite an intensive combination of surgery, radiation and chemotherapy. Although there is an increasing number of 5-year survivors with this combined modality therapy, the median survival remains in the order of 14 months [1]. Pathological studies have demonstrated preferential tumor cell dissemination spread along white matter tracts and brain vessels [2], which limits the efficacy of both microsurgical resection and radiation therapy. The target for post-operative therapeutic radiation after maximal safe resection includes the resection cavity and any residual tumor visible on the postoperative T1-weighted Gadolinium-enhanced MRI. When surgery is not possible due to a high risk of neurological damage, a diagnostic biopsy is undertaken, followed by radiotherapy. To maximise the probability of including relevant microscopic spread from a glioblastoma (glioma WHO grade IV), uniform wide planning margins of up to 30 mm are typically added (Fig. 2B, green line). Some centres further extend this to include all visible edema on the T2-weighted imaging. Recent studies on the pattern of relapse in patients with high-grade glioma (HGG), predominantly glioblastoma, have suggested that tumor recurrence after maximal combined modality therapy occur within 2 cm of the original tumor location [3, 4]. This has led to a suggestion that a

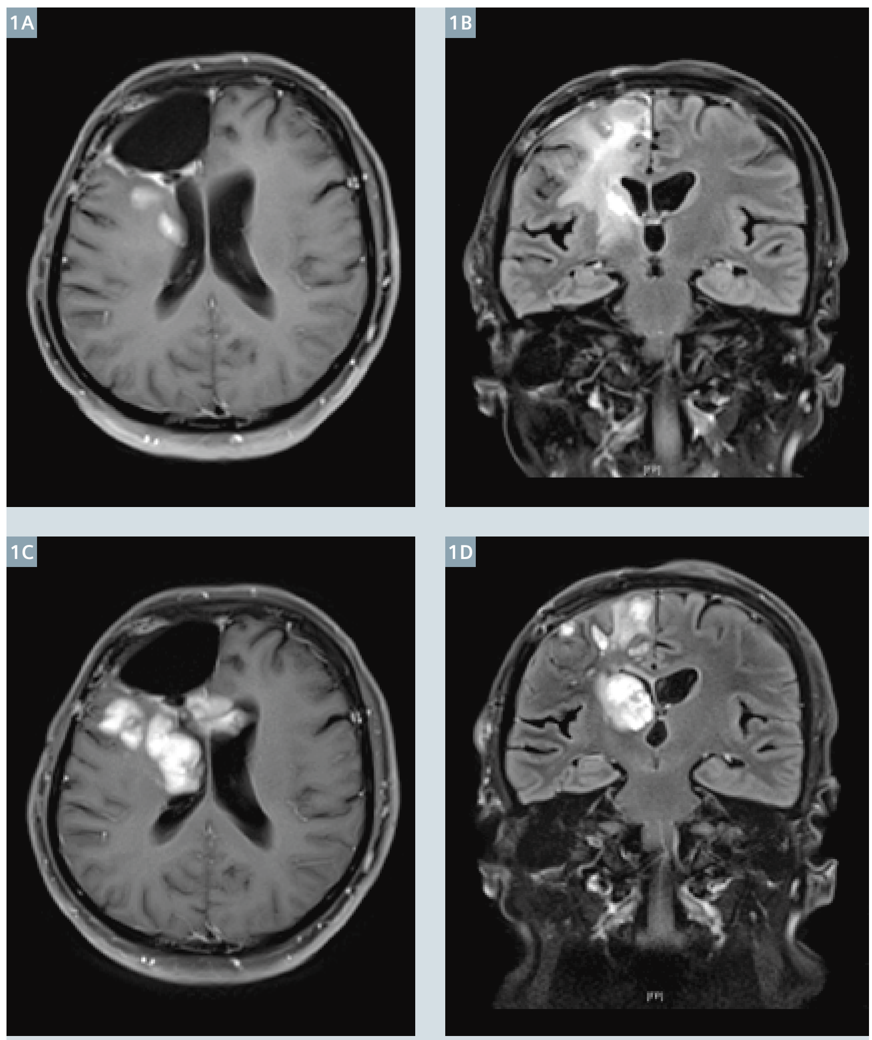


1 Transverse (T1w BLADE fs) and coronal (T2w TIRM dark fluid fs) MR images **(1A, B)** 12 months and **(1C, D)** 16 months after the operation. The patient developed a progressive tumor recurrence contiguous with residual tumor with subsequent extension along neighboring white matter tracts.

reduced margin, for example 1 cm, may be sufficient for the high-dose volume [3].

The addition of temozolomide chemotherapy as a radiation sensitizer and as adjuvant therapy is reported to be associated with an increased risk of normal brain toxicity (radionecrosis) of up to 20% [5]. Radiation-related side effects are dependent on both the prescription dose and the irradiated volume. A dose of at least 60 Gy has been shown to be necessary to control HGG, therefore it is compelling to instead reduce the planning target volume (PTV) where possible without compromising efficacy. Our aim is to derive a biologically targeted volume to ensure coverage of the regions at greatest risk of microscopic infiltration whilst excluding uninvolved brain. To this end, we have explored diffusion tensor imaging (DTI) and fractional anisotropy (FA) to identify areas of tumor infiltration, beyond that visible on T1w contrast-enhanced MRI. The method is derived from the isotropic (p) and anisotropic (q) maps of water diffusivity [6] and based on clinically validated data from patients with HGG [7].

Our technique is best illustrated using a clinical case as an example. This patient with histologically confirmed glioblastoma (GBM), showed tumor progression after surgery and radiation and developed a new lesion in the right thalamus (Fig. 1). The initial pre-operative work-up included DTI to assist the neurosurgeons in the identification and avoidance of apparently uninvolved white matter tracts to minimize the neurological sequelae of the surgery. All the MR imaging was done using a MAGNETOM Avanto 1.5T whole body scanner (Siemens Healthcare, Erlangen, Germany). These same scans were further analysed to extract data

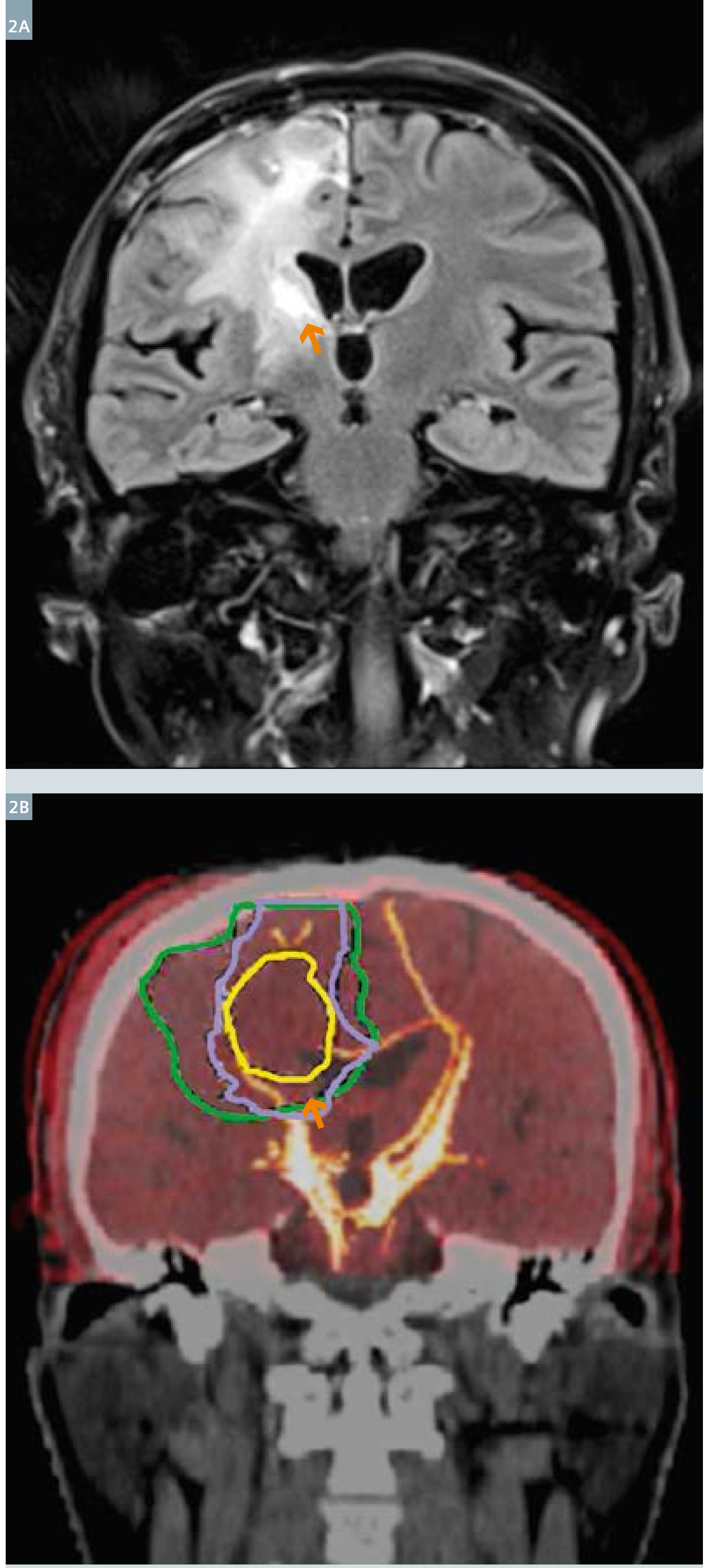


2 Fusion of the MRI at recurrence 12 months post op with the DTI at recurrence 12 months post op suggests a route of spread via the radiologically abnormal right corticospinal tract.

regarding water diffusivity. The initial steps of the radiation planning technique were to co-register the T1w contrast-enhanced MRI with the planning CT scan. The residual enhancing tumor was contoured accordingly and the volume expanded by 1 cm (Fig. 2B, yellow line) to include brain at highest risk of infiltration. In addition, the DTI scan was co-registered and the volume was extended further along the tracts (Fig. 2B, purple line) in contact with the tumor to encompass likely microscopic spread. Any additional regions of tumor and infiltration, as detected by the p and q maps, were delineated and then combined into the target volume by the planning software. This final volume was used to generate intensity modulated radiotherapy (IMRT) plans that were not used for clinical treatment (Fig. 2).

Using an in-house software program, we have developed a technique to incorporate regions of altered water diffusivity, reported to correspond with macroscopic tumor or microscopic infiltration, into the radiotherapy planning process. Conventional large volume irradiation for high-grade glioma carries an inevitable risk of neuro-toxicity, which may be enhanced by combination with radiosensitizers. DTI and FA have previously been reported as diagnostic tools to assist with differential diagnosis, tumor grading, identifying tumor margins and predicting tumor relapse [7-9]. As white matter tracts and alterations in water diffusivity can also be targeted, we believe that future developments in radiation planning for HGG should endeavour to reduce the irradiated volume whilst maintaining adequate coverage of such regions likely to mediate relapse and spread.

### References


1 Stupp R, Hegi ME, Mason WP, van den Bent MJ, Taphoorn MJ, Janzer RC, Ludwin SK, Allgeier A, Fisher B, Belanger K, Hau P, Brandes AA, Gijtenbeek J, Marosi C, Vecht CJ, Mokhtari K, Wesseling P, Villa S, Eisenhauer E, Gorlia T, Weller M, Lacombe D, Cairncross JG, Mirimanoff RO; European Organisation for Research and Treatment of Cancer Brain Tumour and Radiation Oncology Groups; National Cancer Institute of Canada Clinical Trials Group. Effects of radiotherapy with concomitant and adjuvant temozolomide versus radiotherapy alone on survival in gliobastoma in a randomized phase III study: 5-year analysis if the EORTC-NCIC trial. Lancet Oncol. 2009 10(5):459-66.

2 Giese A, Westphal M. Glioma invasion in the central nervous system. Neurosurgery 1996 39(2):235-50.

3 McDonald MW, Shu HK, Curran WJ Jr, Crocker IR. Pattern of failure after limited margin radiotherapy and temozolomide for glioblastoma. Int J RadiatOncol-BiolPhys 2011 1;79(1):130-6.

4 Milano MT, Okunieff P, Donatello RS, Mohile NA, Sul J, Walter KA, Korones DN. Patterns and timing of recurrence after temozolomide-based chemoradiation for glioblastoma. Int J RadiatOncolBiol Phys. 2010 15;78(4):1147-55.

5 Rusthoven KE, Olsen C, Franklin W, KLeinschmidt-DeMasters BK, Kavanagh BD, Gaspar LE, Lillehei K, Waziri A, Damek DM, Chen C. Favorable prognosis in patients with high gradeglioma with radiation necrosis: the University of Colorado experience. Int J Radiat Oncol Biol Phys. 2011 1;81(1):211-7.

6 Basser PJ, Mattiello J, LeBihan D. Estimation of the effective self-diffusion tensor form the NMR spin echo. J MagnReson B 1994 103(3):247-54.

7 Price SJ, Jena R, Burnet NG, Hutchinson PJ, Dean AF,Peña A, Pickard JD, Carpenter TA, Gillard JH. Improved delineation of glioma margins and regions of infiltration with the use of diffusion tensor imaging: an image-guided biopsy study. AJNR Am J Neuroradiol 2006 27(9):1969-74.

8 Byrnes TJ, Barrick TR, Bell BA, Clark CA. Diffusion tensor imaging discriminates between glioblastoma and cerebral metastases in vivo. NMR Biomed 2011 24(1):54-60.

9 Mohsen LA, Shi V, Jena R, Gillard JH, Price SJ. Diffusion tensor invasive phenotypes can predict progression-free survival in glioblastomas. Br J Neurosurg 2013 27 [Epub ahead of print].


## Contact


Jatta Berberat, Ph.D.
Canton Hospital
Tellstrasse
5001 Aarau
Switzerland
jatta.berberat@ksa.ch

# TOGETHER WE MOVE FORWARD IN THE FIGHT AGAINST CANCER

When two leading companies join forces in the fight against cancer, it broadens the realm of what’s possible. That’s why Varian and Siemens have partnered. Siemens' advanced diagnostic imaging capabilities coupled with Varian's powerful delivery systems and treatment planning tools give even more of an edge in the pursuit of our common goal: to **EnVision better cancer care**. Together we offer more personalized treatment and expanded care options that aid you in making the best possible decisions for your patients—with confidence. By gathering our strengths, we have the energy and vision to better help healthcare professionals detect, diagnose and treat cancer while paving the way for the future of cancer care.

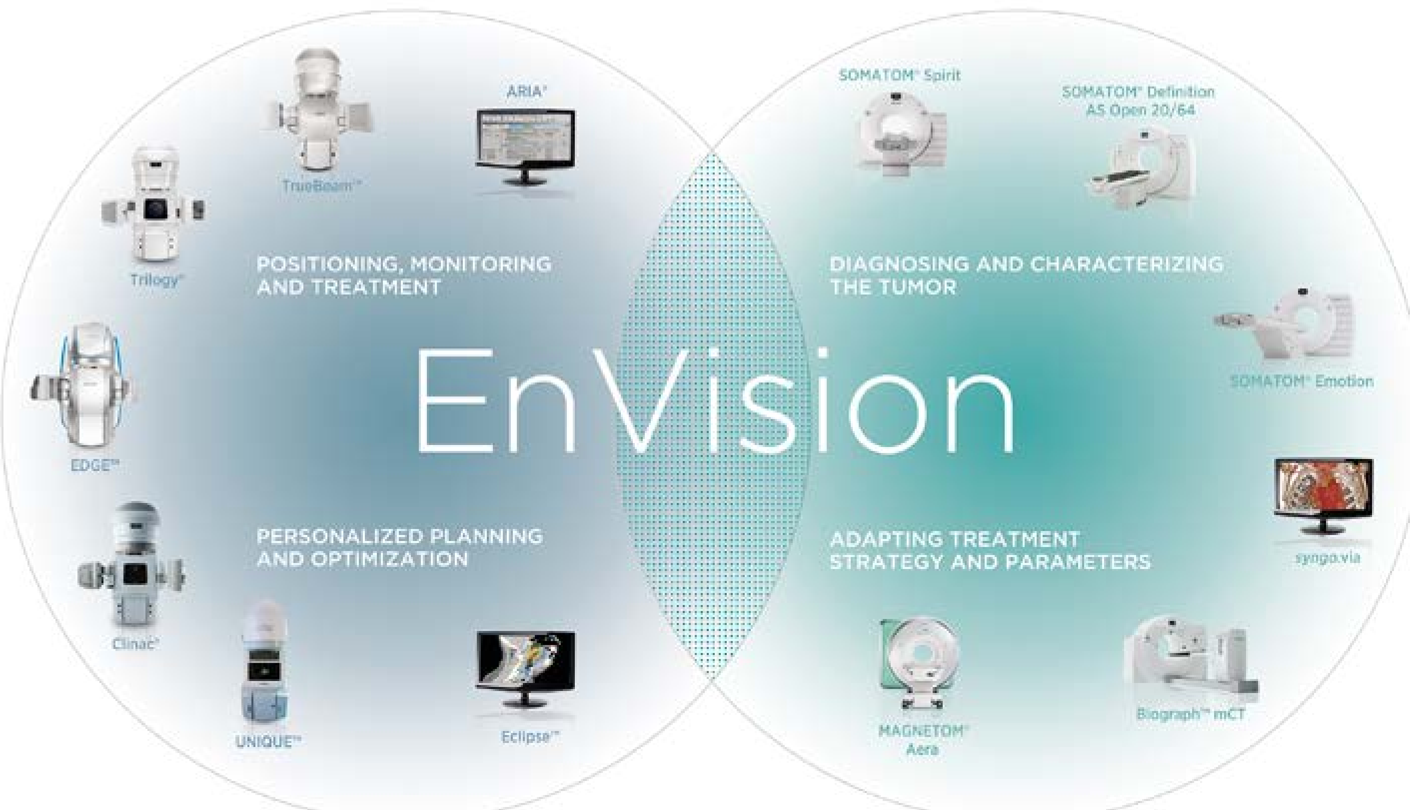


VARIAN
medical systems

SIEMENS
Strategic Partner
of Varian for
Radiation Therapy



Varian Medical Systems
International AG
Zug, Switzerland
Tel: +41 - 41 749 88 44
Fax: +41 - 41 740 33 40
varian.com
info.europe@varian.com

Global Siemens Healthcare
Headquarters
Siemens AG
Healthcare Sector
Henkestrasse 127
91052 Erlangen, Germany
Tel: +49 9131 84-0
siemens.com/healthcare

Find out more at varian.com/envision

# Optimizing MRI for Radiation Oncology: Initial Investigations

**James Balter[1]; Yue Cao[1]; Hesheng Wang[1]; Ke Huang[1]; Shu-Hui Hsu[1]; Martin Requardt[2]; Steven M. Shea[3]**

[1] Department of Radiation Oncology, University of Michigan, Ann Arbor, MI, USA
[2] Siemens Healthcare, Erlangen, Germany
[3] Siemens Corporation, Corporate Technology, Baltimore, USA

## Introduction

The superior soft tissue contrast, as well as potential for probing molecular composition and physiological behavior of tumors and normal tissues and their changes in response to therapy, makes MRI a tempting alternative to CT as a primary means of supporting the various processes involved in radiation therapy treatment planning and delivery. Obvious examples of the benefit of MRI over CT include target delineation of intracranial lesions, nasopharyngeal lesions, normal critical organs such as the spinal cord, tumors in the liver, and the boundaries of the prostate gland and likely cancerous regions within the prostate gland. For brachytherapy planning for cervical cancer, a recent GEC-ESTRO report directly recommends a change from traditional point-based prescriptions based primarily on applicator geometry, to volumetric treatment plans and prescriptions aided by soft tissue visualization, specifically improved by the use of MRI. MRI-based maps of diffusion and perfusion have demonstrated potential for predicting therapeutic outcome for tumors as well as normal tissues, and current clinical trials seek to validate their roles and performance as a means to individualize therapy to improve outcomes (minimize toxicity and improve local tumor control). In addition to these advantages, MRI has been initially investigated as a means to better map the movement and deformation of organs over time and due to physiological processes such as breathing.

The historically accepted challenges in using MRI for primary patient modeling in radiation oncology have included distortion, lack of electron density information, and lack of integrated optimized systems to scan patients immobilized in treatment configuration.

## MRI 'simulator' system

Over the past several years, we have investigated the feasibility of MRI systems to function in the same roles that CT scanners have for the past 10–15 years, that is as primary tools for patient modeling for radiation therapy. These efforts have accelerated in the past years with the installation of a dedicated MRI 'simulator' at the University of Michigan, based on a 3T wide-bore scanner (MAGNETOM Skyra, Siemens Healthcare, Erlangen, Germany), outfitted with a laser marking system (LAP, Lueneburg, Germany) and separate detachable couch tops supporting brachytherapy and external beam radiation therapy applications.

1A

1B

**1** MRI simulation system shows a volunteer in position for initial setup wearing a customized face mask **(1A)**. Close-up view of anterior coil setup and crosshairs from laser marking system **(1B)**.

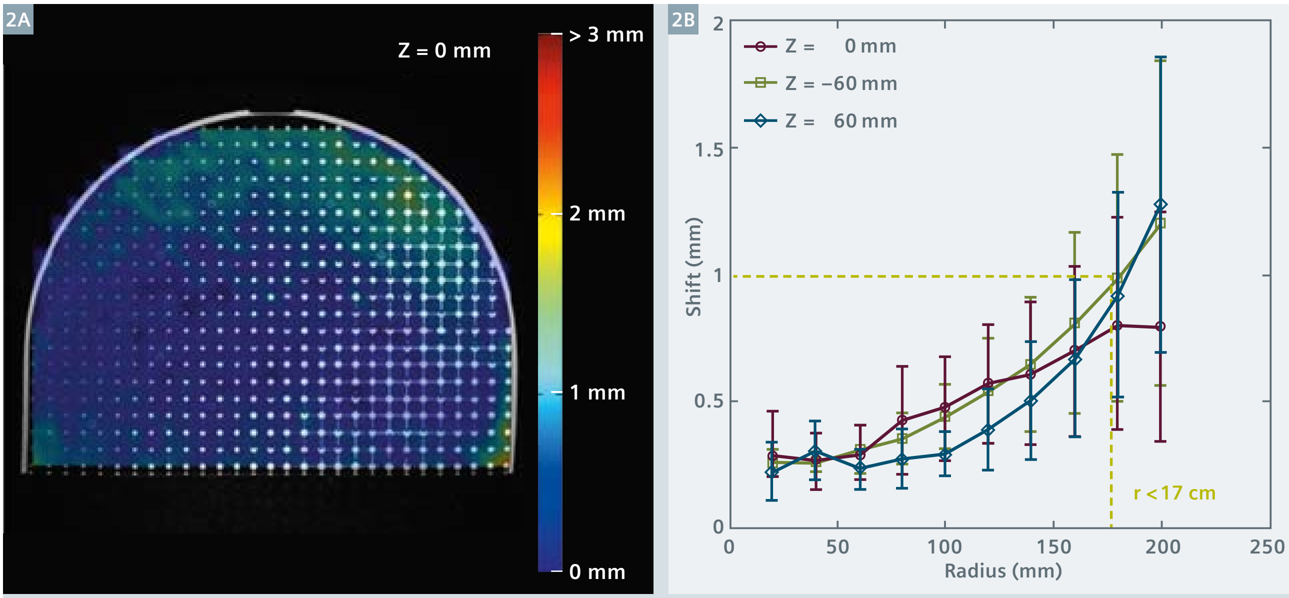


2 Colorwash of measured distortion through an axial plane of the distortion phantom **(2A)**. Magnitude of distortion-induced shifts in circles of increasing radius from the bore center in axial planes at the center and +/– 6 cm along the bore **(2B)**.

The process of integrating MRI into the standard workflow of radiation oncology requires attention be paid to a number of specific areas of system design and performance. In our instance, we chose a system that could potentially support both external beam therapy as well as brachytherapy. The brachytherapy requirement played a specific role in some of our design choices. As the high-dose-rate (HDR) brachytherapy system was housed in a room across the hall from the MRI suite, a room design was created that permitted the direct transfer of patients from MRI scanning to treatment. Typically brachytherapy treatment has involved transferring patients to and from imaging systems, a process that could potentially influence the treatment geometry and changes the dose delivered away from that planned. Treating a patient directly without moving them has significant advantages for geometric integrity as well as patient comfort. To facilitate such treatments, a detachable couch was chosen as part of the magnet specifications, and two such couches were specifically purchased to support simultaneous treatment of patients on the couch used for MRI scanning and scanning of other patients for subsequent external beam treatments.

To support external beam radiotherapy, patients need to be scanned in positions and configurations that can be reproduced at treatment. In addition to necessitating a wide bore MRI scanner, an indexed flat table top insert was purchased from a company that specializes in radiation therapy immobilization systems (Civco, Kalona, IA, USA). A number of immobilization accessories were customized for use in the MRI environment, most notably a head and neck mask attachment system. To support high quality scanning of patients in treatment position without interfering with their configuration for treatment, a series of attachments to hold surface coils (primarily 18-channel body coils) relatively close to the patient without touching are used.

## Initial commissioning and tests

To commission the system, a number of tests were performed in addition to the standard processes for MRI acceptance and quality assurance. The laser system was calibrated to the scanner coordinates through imaging of a phantom with externally visible laser alignment markings and internal MRI-identifiable coordinates indicating the nominal laser intersection, and end-to-end tests were performed on phantoms and volunteers to establish the accuracy of isocenter marking using MRI scans as a source of input.

To characterize system-level distortion, a custom phantom was developed to fill the bore of the magnet (with perimeter space reserved for testing the 18-channel body coil if desired). The resulting phantom was a roughly cylindrical section with a sampling volume measuring 46.5 cm at the base, with a height of 35 cm, and a thickness of 16.8 cm. This sampling volume was embedded with a three-dimensional array of interconnected spheres, separated by 7 mm center-to-center distances. The resulting system provided a uniform grid of 4689 points to sample the local distortion. The phantom was initially scanned using a 3D, T1-weighted, spoiled gradient echo imaging sequence (VIBE, TR 4.39 ms and TE 2.03 ms, bandwidth 445 Hz/pixel) to acquire a volume with field-of-view of 500 × 500 × 170 mm with a spatial resolution of 0.98 × 0.98 × 1 mm. Standard 3D shimming was used for scanning, and 3D distortion correction was applied to the images prior

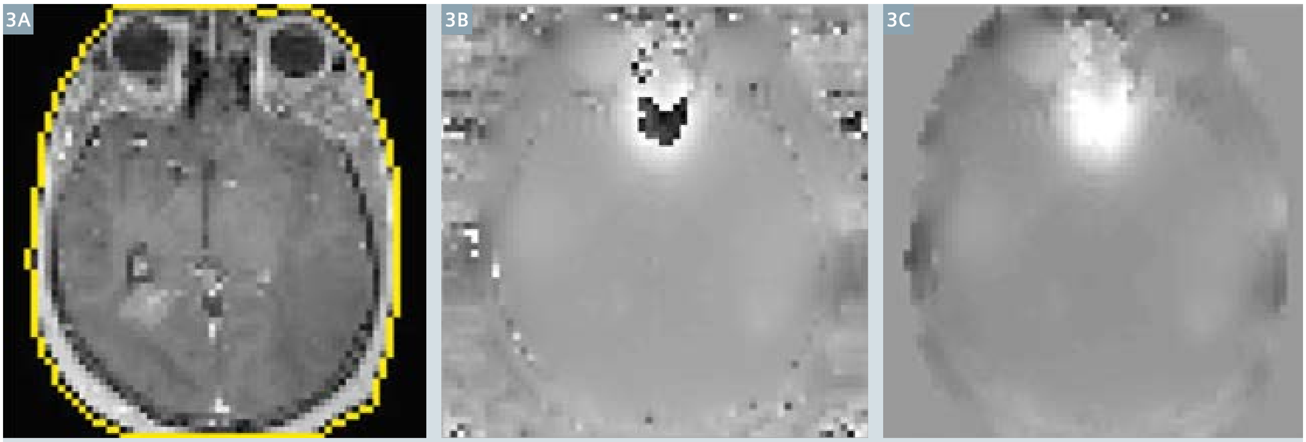


3 T1-weighted image with external contour delineated as a mask **(3A)**. The $B_0$ inhomogeneity map acquired from this subject **(3B)** was unwrapped within the boundaries of the mask, yielding the resulting distortion map **(3C)**.
*Reprinted with permission from Wang H, Balter J, Cao Y. Patient-induced susceptibility effect on geometric distortion of clinical brain MRI for radiation treatment planning on a 3T scanner. Phys Med Biol 58(3):465-77, 2013.*

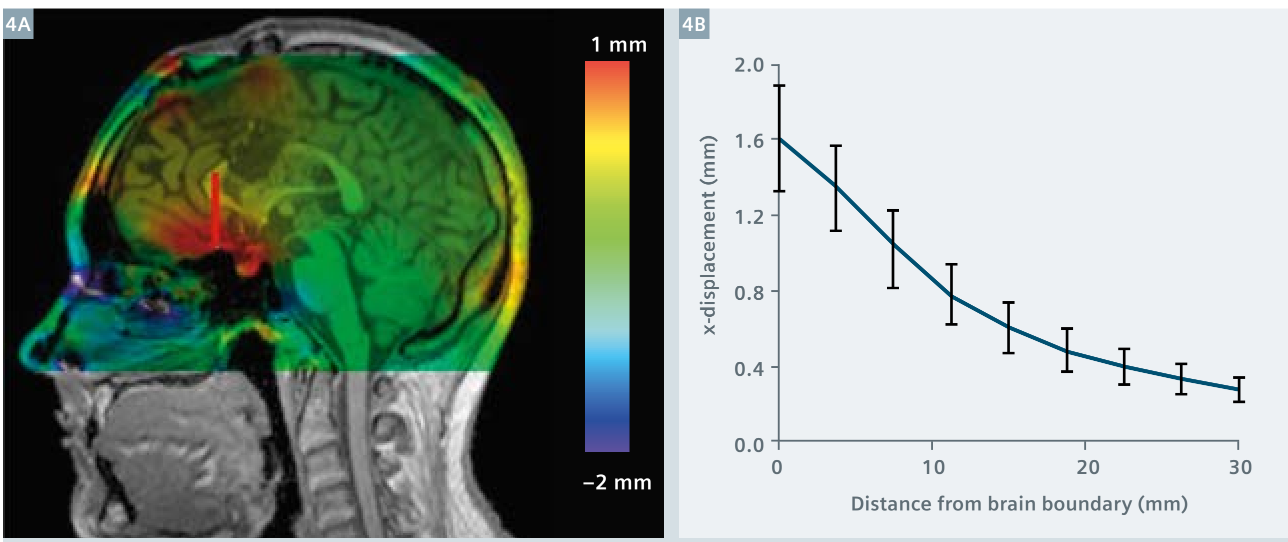


4 Colorwash of distortion-induced displacements through a sagittal plane of a subject **(4A)**. Analysis of displacements along a line moving away from the sinus (red line in fig. 4A) shows the falloff of distortion due to susceptibility differences as a function of distance from the interface **(4B)**.
*Reprinted with permission from Wang H, Balter J, Cao Y. Patient-induced susceptibility effect on geometric distortion of clinical brain MRI for radiation treatment planning on a 3T scanner. Phys Med Biol 58(3):465-77, 2013.*

to analysis. For this initial test, the body coil integrated into the magnet was used. Automated analysis of the images localized the sphere centers, yielding a deformation vector field that described the influence of system-level distortion on the measured sphere locations. This initial test demonstrated the accuracy of coordinate mapping via this scanning protocol, with average 3D distortions of less than 1 mm at radii of up to 17 cm in planes through the bore center as well as +/– 6 cm along the bore length. Of note, scanning was performed using the *syngo* MR D11 software version. Future tests will be performed on the *syngo* MR D13 release.

To begin to assess the impact of subject-induced susceptibility on distortions, $B_0$ inhomogeneity maps were acquired during routine patient scanning and analyzed (for 19 patients) under an IRB-approved protocol. These maps were acquired using a 2D, double-echo, spoiled gradient echo sequence (GRE field mapping $TE_1$ 4.92 ms, $TE_2$ 7.38 ms, TR 400 ms, flip angle 60 degrees, voxel size 3.5 × 3.5 × 3.75 mm), masked by the boundaries of the head acquired from T1-weighted images, and unwrapped using an algorithm from the Oxford Center for Functional Magnetic Resonance Imaging of the Brain [1]. The resulting maps showed homogeneity

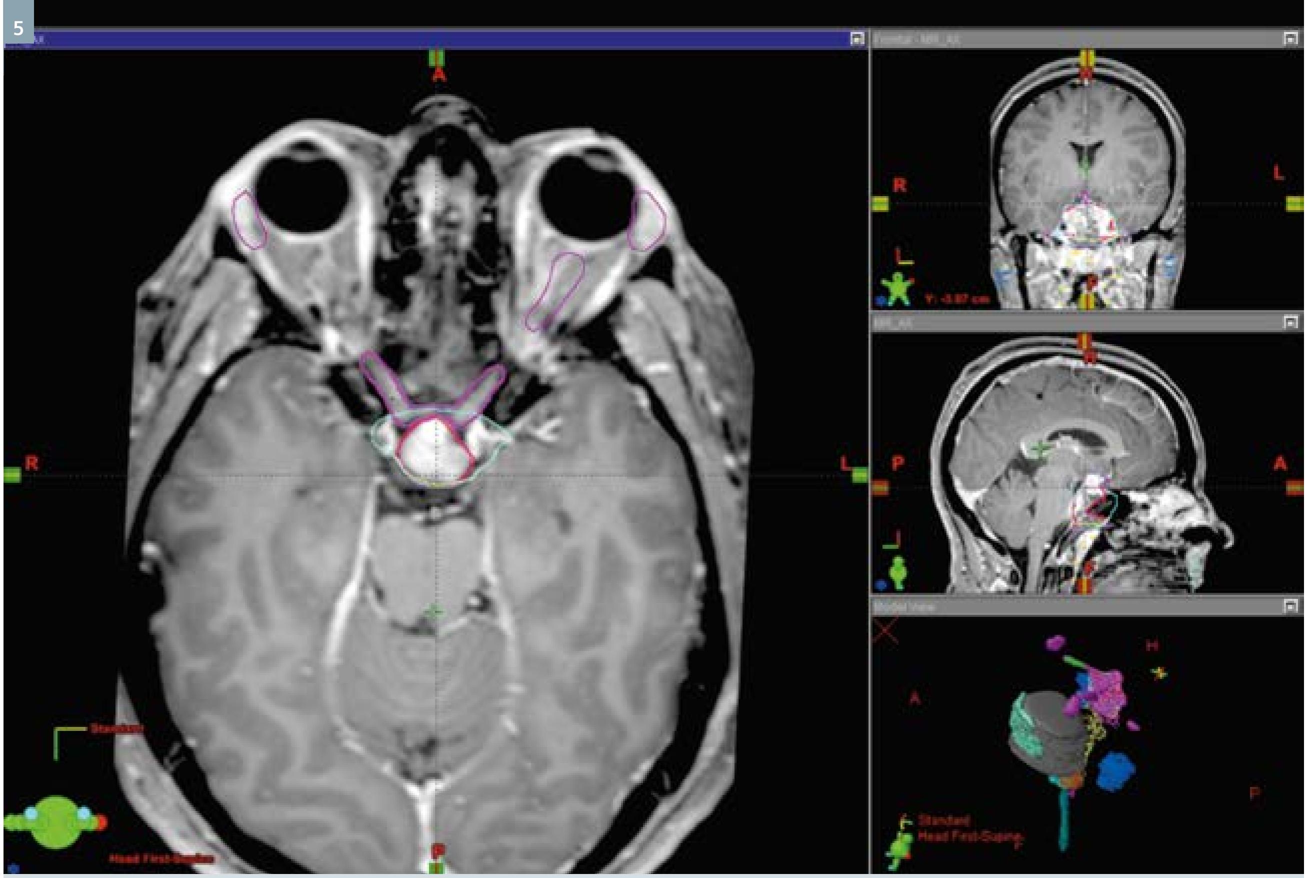


5 Post-contrast T1-weighted images of a patient scanned in an immobilization mask using an anterior 18-channel body surface coil and a posterior 4-channel small soft coil and displayed in a radiation therapy treatment planning system (Eclipse, Varian, Palo Alto, CA, USA). Various delineated structures shown are used to guide optimization of intensity-modulated radiation therapy.

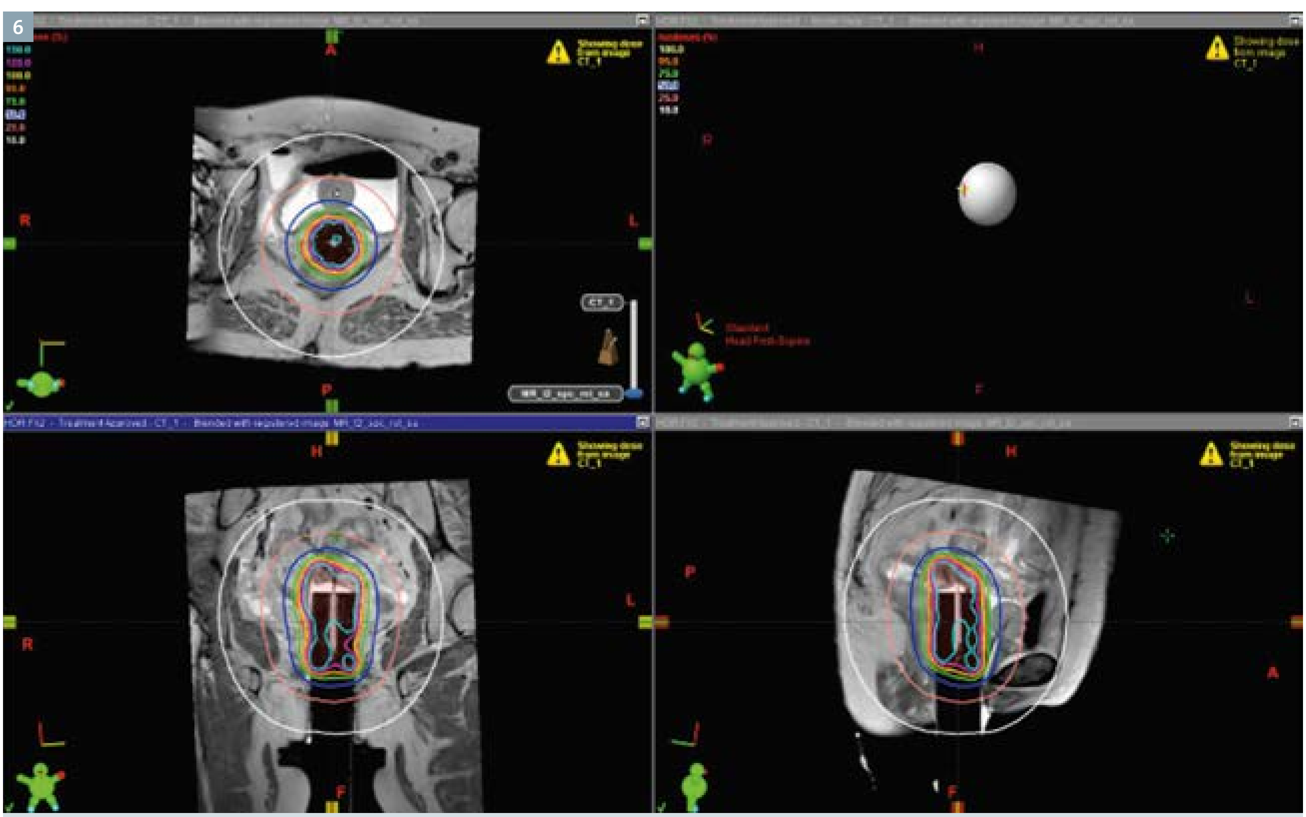


6 Display from a brachytherapy treatment planning system (Brachyvision, Varian, Palo Also, CA, USA) showing orthogonal planes through cylindrical applicator implanted in a patient. Source locations (red dashes through the center of the applicator) are shown, as well as radiation isodose lines.

of 0.035 ppm or less over 88.5% of a 22 cm diameter sphere, and 0.1 ppm or less for 100% of this volume.

These inhomogeneity maps were applied to calculate distortions from a typical clinical brain imaging sequence (3D T1-weighted MPRAGE sequence with TE 2.5 ms, Siemens TR 1900 ms, TI 900 ms, flip angle 9 degrees, voxel size 1.35 × 1.35 × 0.9 mm, frequency-encoding sampling rate of 180 Hz/pixel). On these images, 86.9% of the volume of the head was displaced less than 0.5 mm, 97.4% was displaced less than 1 mm, and 99.9% of voxels exhibited less than 2 mm displacement. The largest distortions occurred at interfaces with significant susceptibility differences, most notably those between the brain and either metal implants or (more significantly) adjacent air cavities. In the location with the largest displacement (interface with the sinus), the average displacement of 1.6 mm at the interface falls to below 1 mm approximately 7 mm away.

## Examples of clinical use

We have implemented a number of scanning protocols in our first year of operation. Routine scans are performed for patients with intracranial lesions of all forms, as well as for those with nasopharyngeal tumors, hepatocellular carcinoma, and certain spinal and pelvic lesions. Routine use of the system for MRI-based brachytherapy of patients with cervical cancer using a ring and tandem system is currently pending modification of part of the applicator for safety and image quality reasons, although patients undergoing other implants (e.g. cylinders) have had MRI scans to support treatment planning.

## Summary

We have implemented the initial phase of MRI-based radiation oncology simulation in our department, and have scanned over 300 patients since operations began just over one year ago. The system demonstrates sufficient geometric accuracy for supporting radiation oncology decisions for external beam radiation therapy, as well as brachytherapy. Work is ongoing in optimizing MRI scanning techniques for radiation oncology in various parts of the body and for various diseases. In addition to current and future work in optimizing MRI for use in routine radiation therapy, a variety of research protocols are underway using this system. A major current focus is on using MRI without CT for external beam radiation therapy. Results of these efforts will be presented in future articles.

### References


1 Jenkinson M. Fast, automated, N-dimensional phase-unwrapping algorithm. Magn Reson Med. 2003 Jan;49(1):193-7.

2 Dimopoulos JC, Petrow P, Tanderup K, Petric P, Berger D, Kirisits C, Pedersen EM, van Limbergen E, Haie-Meder C, Pötter R. Recommendations from Gynaecological (GYN) GEC-ESTRO Working Group (IV): Basic principles and parameters for MR imaging within the frame of image based adaptive cervix cancer brachytherapy. Radiother Oncol 103(1):113-22, 2012.

3 Wang H, Balter J, Cao Y. Patient-induced susceptibility effect on geometric distortion of clinical brain MRI for radiation treatment planning on a 3T scanner. Phys Med Biol 58(3):465-77, 2013.


## Contact


James M. Balter, Ph.D., FAAPM
Professor and co-director,
Physics division
Department of Radiation Oncology
University of Michigan
Ann Arbor, MI
USA
Phone: +1(734)936-9486
jbalter@umich.edu

# Management of MRI Spatial Accuracy for Radiation Therapy

Teo Stanescu, Ph.D.; David Jaffray, Ph.D.

Princess Margaret Cancer Centre, University Health Network; Department of Radiation Oncology, University of Toronto, Toronto, ON, Canada

## Introduction

Radiation Therapy (RT) demands tight constraints regarding the geometric accuracy of image data used in its workflows for treatment simulation and in-room treatment delivery guidance. The spatial accuracy requirements are largely driven by the ability to deliver and deposit therapeutic radiation doses to targeted anatomical sites (1-2 mm). The benefits of MRI's superior soft-tissue contrast as compared to RT's gold standard based on x-ray imaging (i.e. CT, Cone Beam CT) are somewhat overshadowed by the intrinsic MR image distortions manifested as loss of spatial accuracy and local intensity inhomogeneities.

The MR image distortions are given by a) scanner-related distortions caused by nonlinearities in the imaging gradients and inhomogeneities in the main magnetic field ($B_0$), and b) patient-induced distortions mainly due to variations in the magnetic susceptibility properties of neighboring tissues (and chemical shift). The scanner-related distortion field ($S$) is predictable, independent of the imaged subject and its spatial characteristics are static over time given optimal functionality of the MR system. $S$ magnitude is negligible in the vicinity of the MR isocenter and gradually increases with distance, reaching about 1-2 cm for large fields of views [1-3]. In comparison, the susceptibility-induced distortion field ($X$) is highly dependent on the subject anatomy as they arise at the boundary between structures exhibiting local discontinuities in the susceptibility ($\chi$) values, e.g. soft-tissue and air-filled cavities. The magnitude of $\chi$ effects is in the range of a few millimeters and depends on several factors such as magnetic field and encoding gradient strength [4, 5].

A composite distortion field ($C$) can be defined as the vector summation of $S$ and $X$, to characterize the combined aspects of the two fields [6]. $S$ and $X$

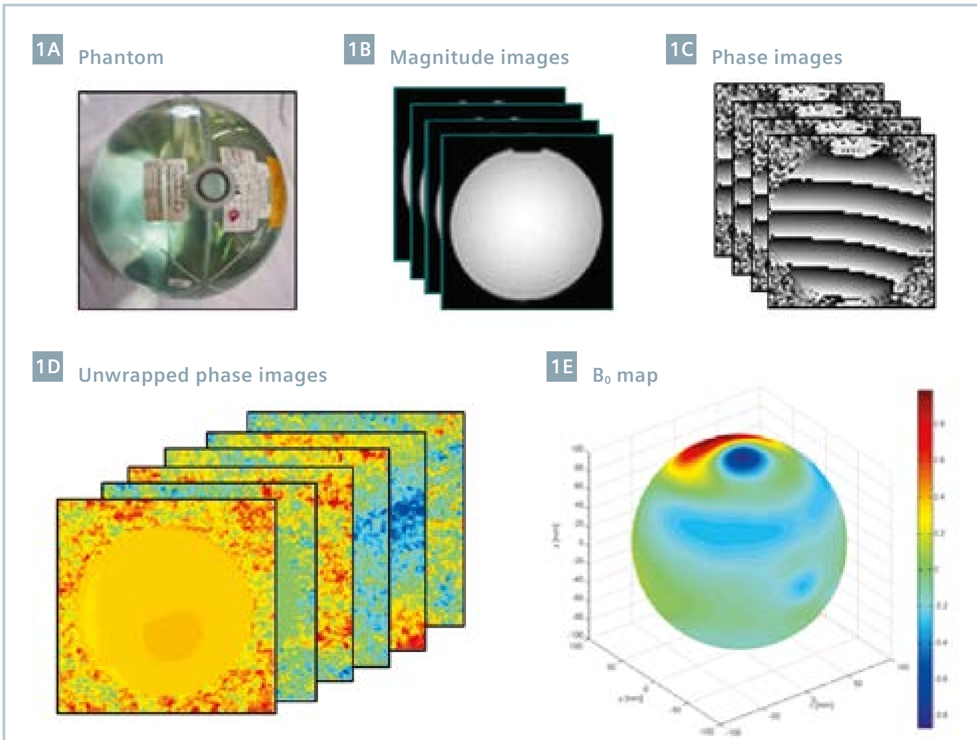


1 $B_0$ mapping: the magnitude images of a spherical uniformity phantom are used to facilitate the segmentation and analysis of the phase images. The 3D distribution of the magnetic field is then computed from the unwrapped phase images and $B_{rms}$ and $B_{pp}$ values are derived to quantify the overall field homogeneity. Visualization of the 3D map is also provided for trouble-shooting purposes.

have negligible mutual coupling and can be treated independently following dedicated methodology. When $C$ is associated with intrafraction motion, specific to mobile anatomical structures, it becomes more complex featuring 4D characteristics, e.g. for fast imaging 2D-cine, 4D MR. The quantification of $C$ is then particularly challenging due to real anatomical changes in the targeted structure's volume, shape and relative location within the MR imaging volume. The accurate knowledge of a tumor's true contours during the motion cycle is paramount for advanced RT planning and delivery techniques which are based on radiation field gating or tracking [7, 8].

MR manufacturers made significant progress over the past years in implementing improved hardware and algorithms to reduce the magnitude of $S$. However, residual distortions are still an issue for RT applications [9]. Overall, the geometric distortions need to be well-understood for each MR-based technique and appropriate mitigation implemented to safely integrate MR data in radiotherapy workflows. Our work on the management of MR image distortions is motivated by the clinical implementation of MR-guided brachytherapy and external beam RT technologies and to enable MR-based adaptive procedures [10].

## Scanner-related distortions

Routine testing for monitoring the field homogeneity and its stability is recommended as a pre-requisite for good imaging. As part of our standard procedures for MR commissioning and periodic quality control (QC) of the system shim, we develop and implemented a fast $B_0$ mapping technique based on a) phantom data acquisition with a GRE double-echo sequence and b) an image processing algorithm for data reformatting and phase unwrapping, and c) generation of analytics and reporting. The simplified flowchart is shown in Figure 1. First, magnitude and phase images are collected with a uniformity phantom. Then phase unwrapping is performed using the PUROR method [11] and metrics such as $B_{rms}$ (root mean square) and $B_{pp}$ (peak-to-peak) are computed and reported in a ready to print file. The image acquisition and post-processing was optimized to match the performance of the Phantom Shim Check procedure available in the Siemens service environment (1.5T MAGNETOM Espree, with software version *syngo* MR B17A). The total time to scan and run the analysis on a mid-range PC workstation is under 100 seconds.

It is typical to quantify the gradient nonlinearities using a) a theoretical approach considering the spherical harmonics coefficients specific to each gradient set or b) via measurements with a linearity phantom. Although the theoretical approach is very appealing as it can be easily streamlined for image unwarping of live image data, it does not fully compensate for the image geometric errors [3, 9]. A phantom with a known structure, the most common being a 2D or 3D grid pattern, is desirable to measure the remainder of the distortions. In RT one of the requirements is to accurately define the anatomy for both small and large field of views, which means that the linearity phantoms should be able to provide enough spatial coverage. In particular, at large FOVs a phantom with a grid pattern needs to fill the entire volume to provide adequate sampling for $S$, which often translates into increased phantom weight. The manufacturing, routine preparation (positive or negative contrast) and manipulation of such a phantom may also be challenging.

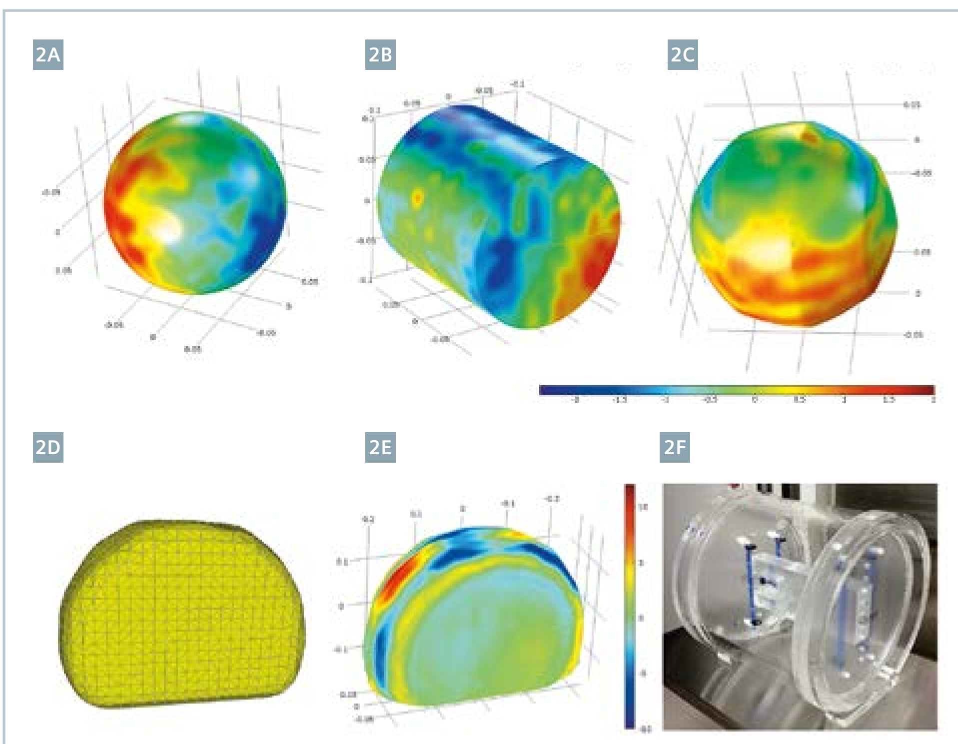


2 Harmonic analysis was applied to compute the 3D distortion vector field for an arbitrarily shaped volume from data measured on the surface. **(2A)** and **(2B)** show basic quadratic geometries; **(2C)** shows a Reuleaux 9-gon to test the method for a more complex structure; **(2D)** depicts the meshed and irregular surface of an MR imaging FOV as measured with a large phantom based on a grid design; **(2E)** the surface data corresponding to **(2D)** was used as BC in the harmonic analysis to stress-test its performance.

To address the above limitations our group focused on a design which minimized phantom material, weight and implicitly the manufacturing cost without compromising the accuracy in quantifying $S$. The design was driven by the ability to fully reconstruct $S$ in a given volume solely from field data mapped on the geometry's surface [12]. This means that harmonic analysis can be applied to $S$, since $S$ is natively related to the magnetic field. Specifically, the Laplace equation was solved with well-defined Dirichlet boundary conditions (BC) for functions representing the 3D geometric distortion vector field. The Dirichlet BCs were given by the measured vector field values corresponding to the domain's boundary. The method was validated for multiple quadratic and arbitrary geometries. In particular, Figure 2E depicts sample results for a general case of a highly irregular surface, which wraps the raw data measured on a grid phantom with a high density of control points. The case is challenging due to the magnitude and local gradients specific to $S$ at large FOVs. A cylindrical shell phantom and associated software application based on the harmonic analysis was developed in collaboration with Modus Medical Devices (London, ON, Canada) as shown in Figure 2F [13].

## Susceptibility-induced distortions

The field $X$ is challenging to predict or quantify, especially when live image data is needed for the clinical decision making process. The map of tissue susceptibility-induced effects may change even for the same patient as a function of daily anatomy. Several methods were proposed in the literature to assess the $\chi$ perturbations [5, 4, 15]. Rather than measure the susceptibility, which often requires additional image data leading to longer acquisitions times, we chose to investigate the $\chi$ effects by means of numerical simulations [4, 6]. A finite difference technique iteratively solves the Maxwell equations with associated BCs for the case of a time independent and uniform magnetic field (i.e. $B_0$ of an MR scanner). The input data is given by 3D susceptibility maps synthetically generated by assigning bulk $\chi$ values to anatomical structures delineated on CT image data sets. CT images were used to ensure the spatially true representation of the anatomy and to dissociate the $\chi$ effects from other potential sources of geometric inconsistencies (e.g. $B_0$ and $B_1$ local inhomogeneities, $S$). Magnetic field maps expressed in terms of ppm values were set as the output of the numerical computations. The spatial distortions (in mm) were then easily converted by specifying the $B_0$ and readout gradient values ($\Delta_{mm}=ppm\cdot B_0/G_E$). Furthermore, the $\Delta_{mm}$ values were interpolated and reported for the anatomical regions of interest. The simulation method was validated in phantom using a wide range of $G_E$ values at 1.5T and 3T.

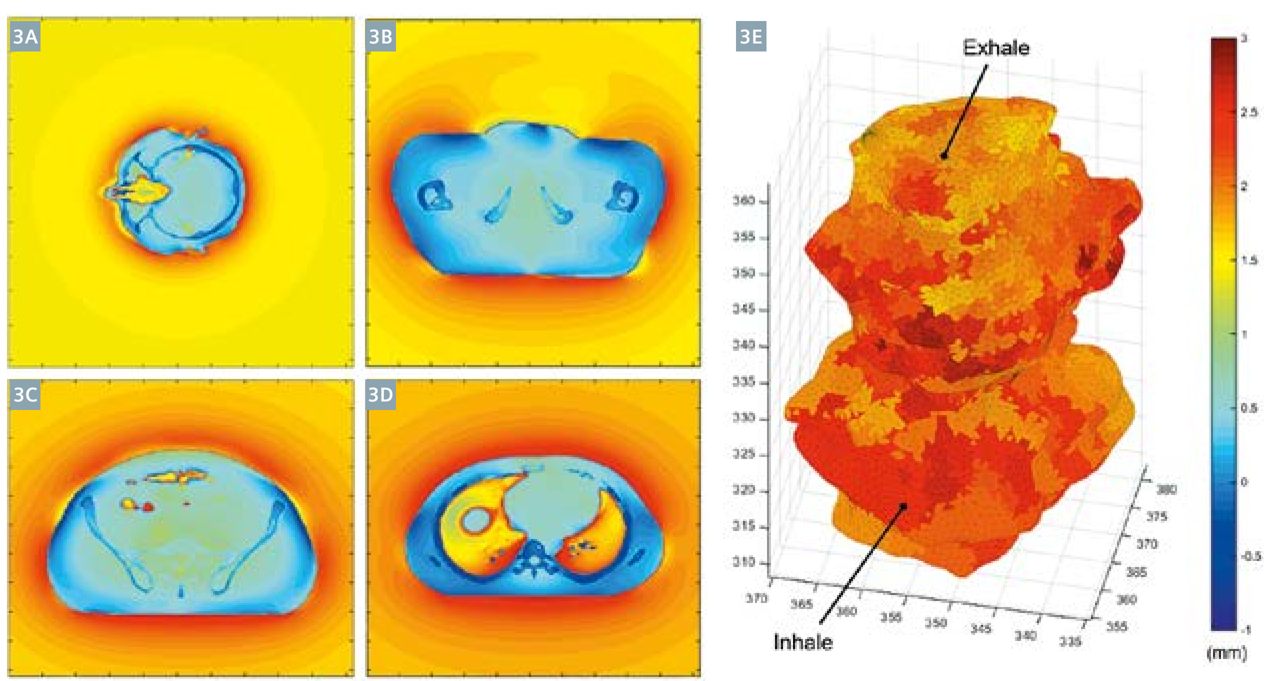


3 Sample results of the magnetic field numerical computations performed to investigate the magnitude of $\chi$ geometric effects. Multiple anatomical regions were simulated such as **(3A)** brain (whole skull), **(3B)** prostate, **(3C)** abdomen/upper GI, and **(3D)** lung. Inset **(3E)** shows the 4D composite distortion field results for a small and mobile lung tumor as estimated for the two extreme phases of the respiratory cycle, i.e. inhale and exhale.

Figure 3 shows several examples of $\chi$ as modelled for specific anatomical sites. We found the data useful for at least two reasons: a) estimate the maximum boundary of the $\chi$ effects for a given site and b) generate $\Delta_{mm}=f(G_E)$ curves for $B_0$ values of interest. The trends from b) were used to guide the optimization of clinical imaging protocols so that the geometric distortions were mitigated while the SNR penalty for increasing $G_E$ was minimized. Therefore, our approach was to predict the $\chi$ effects outcome for patient populations and compensate upfront whenever possible.

## 4D Composite distortion field

The raw MR images intrinsically embed the effects of both scanner-related and $\chi$-induced geometric distortions. The assessment of $C$ for mobile tumors may be particularly non-trivial due to continuous variations in the local profile of the $S$ and $\chi$ fields as experienced by the tumors [6]. For example, $S$ is static with respect to the MR scanner, but when seen from the mobile tumor's system of reference it becomes time-dependent as the target travels in regions with potentially different local $S$ values. Therefore, a 4D characteristic may be associated with $S$. Similarly, $\chi$ becomes 4D as the tumor deforms and changes location relative to surrounding anatomical landscape. To evaluate the upper boundary of the 4D composite field we combined the methodologies from above for $S$ and $\chi$ in the case of mobile lung tumors. The susceptibility simulations were performed for 10 separate 3D data sets representing individual phases of the breathing cycle as captured with 4D CT imaging. $S$ was also derived for all tumor motion phases via vector field interpolation. Metrics such as max/mean/range and spatial perturbations in the tumor's center of mass were reported for the individual and combined fields. An example is shown in Figure 3E. The dominant contribution was from $S$, and it was suggested that a unique $C$ correction (e.g. derived from one phase or a mean phase) may be applied to all tumor phases with negligible residual errors. For fast imaging, $\chi$ was found largely negligible as a high BW is typically employed.

## Summary

The quantification of geometric distortions is needed especially for radiation therapy applications to ensure a high degree of image data accuracy. Knowing the true location of the targeted anatomy may enable the use of tighter treatment margins expected to improved tumor control through dose escalation and increased sparing of healthy tissues. The assessment of MR image distortions is recommended to be part of the MR scanner commissioning and routine quality control. The susceptibility effects may be minimized within acceptable thresholds in certain applications whereas the scanner-related distortions may be mapped via phantoms and unwrapped on patient data when relevant.


### References

1 D. Wang, W. Strgnell, G. Cowin, D.M. Doddrell, R. Slaughter, "Geometric distortion in clinical MRI systems Part II: correction using a 3D phantom," Magn. Reson. Imag. 22(9):1223-32 (2004).

2 S.F. Tanner, D.J. Finnigan, V.S. Khoo, P. Mayle, D.P. Dearnaley, M.O. Leach, "Radiotherapy planning of the pelvis using distortion corrected MR images: the removal of system distortions," Phys. Med. Biol. 45:2117-2132 (2000).

3 S.J. Doran, L. Charles-Edwards, S.A. Reinsberg, M.O. Leach, "A complete distortion correction for MR images: I. Gradient warp correction," Phys. Med. Biol. 50(7):1343-61 (2005).

4 T. Stanescu, K. Wachowicz, D.A. Jaffray, "Characterization of tissue magnetic susceptibility-induced distortions for MRIgRT," Med. Phys. 39(12):7185-93 (2012).

5 R. Bhagwandien, M.A. Moerland, C.J.G. Bakker, R. Beersma, J.J.W. Lagendijk, "Numerical analysis of the magnetic field for arbitrary magnetic susceptibility distributions in 3D," Mag. Res. Imag. 12:101-107 (1994).

6 T. Stanescu, D. Jaffray, "Investigation of the 4D composite MR image distortion field associated with tumor motion for MR-guided radiotherapy," Med. Phys. (in press).

7 M.B. Tacke, S. Nill, A. Krauss, U. Oelfke, "Real-time tumor tracking: automatic compensation of target motion using the Siemens 160 MLC," Med. Phys. 37(2):753-61 (2010).

8 A. Sawant, R.L. Smith, R.B. Venkat, L. Santanam, B. Cho, P. Poulsen, "Toward submillimeter accuracy in the management of intrafraction motion: the integration of real-time internal position monitoring and multileaf collimator target tracking," Int. J. Radiat. Oncol. Biol. Phys. 74(2): 575-82 (2009).

9 A. Walker, G. Linley, P. Metcalf, L. Holloway, "MRI distortion: considerations for MRI based radiotherapy treatment planning," Austral. Phys. Engin. Sci. Med. 37(1):103-113 (2014).

10 D. Jaffray, M. Carlone, M. Milosevic, S. Breen, T. Stanescu, "A facility for magnetic resonance-guided radiation therapy," Semin. Radiat. Oncol. 24(3):193-5 (2014).

11 J. Liu, M. Drangova, "Intervention-based multidimensional phase unwrapping using recursive orthogonal referring," Magn. Reson. Med. 68(4):1303-16 (2012).

12 T. Tadic, D. Jaffray, T. Stanescu, "Harmonic analysis for the characterization and correction of geometric distortion in MRI," Med. Phys. 41(11):112303 (2014).

13 http://modusqa.com/imaging/phantoms/mrid3d

14 H. Chang and J. Fitzpatrick, "A technique for accurate magnetic resonance imaging in the presence of field inhomogeneities," IEEE Trans. Med. Imaging 11, 319–329 (1992).

15 M. Jenkinson, J. L. Wilson, and P. Jezzard, "Perturbation method for magnetic field calculations of nonconductive objects," Magn. Reson. Med. 52(3), 471–477 (2004).


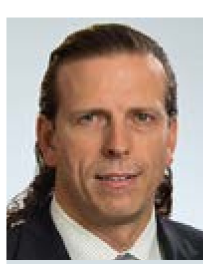

Dr. David Jaffray

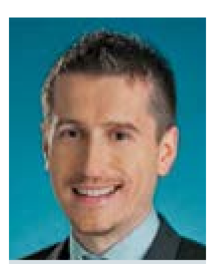

Dr. Teo Stanescu

## Contact


Teo Stanescu, PhD, MCCPM
Assistant Professor
Princess Margaret Cancer Centre
610 University Avenue
Toronto, ON, M5G 2M9
Canada
Phone (416) 946-4501 Ext. 5071
teodor.stanescu@rmp.uhn.ca

# Benefits of Time-Correlated and Breath-Triggered MR Acquisition in Treatment Position for Accurate Liver Lesion Contouring in Stereotactic Body Radiotherapy

Soléakhéna Ken, Ph.D.[1]; Richard Aziza, M.D.[3]; Aurélie Tournier, MSc[1]; Michel Rives, M.D.[2]; Françoise Izar, M.D.[2]; Younès Sekkal, BSc[3]; Nicolas Morel, BSc[3]; Laure Parent, Ph.D.[1]

[1] Institut Universitaire du Cancer Toulouse Oncopôle, Engineering and medical physics department, Toulouse, France
[2] Institut Universitaire du Cancer Toulouse Oncopôle, Radiotherapy department, Toulouse, France
[3] Institut Universitaire du Cancer Toulouse Oncopôle, Imaging department, Toulouse, France

## Introduction

In stereotactic body radiotherapy (SBRT), high-gradient dose is delivered and target volumes have to be delineated precisely in order to avoid irradiation of healthy tissue. Liver lesions are not always visible on planning CT imaging, even after injection of contrast agent. MR images are therefore necessary for a precise lesion contouring. Accurate registration is thus a crucial step for SBRT planning in order to perform relevant delineation of target volumes.

Prior to imaging, gold fiducials are implanted under echo or CT guidance inside or in the vicinity of the lesions. These fiducials are used both as surrogate to pinpoint the lesion in order to precisely position the patient on the treatment machine, and also as markers to register planning CT and MR images.

Liver imaging is challenging because of movement caused by breathing. This movement has been reported to be up to 2 cm in free breathing [1]. Our institution uses audio coaching for a better breathing pattern reproducibility [2].

In order to account for breathing motion, planning CT is performed on a 4D CT. The planning and treatment are generally made on exhale images as these are more reproducible [3]. MR sequences were thus optimized to match CT images in exhale phase.

## MR imaging

With the aim of improving registration accuracy, MR images were acquired in the same position as for CT planning images using Orfit (Orfit Industries, Wijnegem, Belgium) dedicated thermo-plastic nets, table, supports and cushions and Civco (Civco Medical Solutions, Coralville, Iowa, USA) knee cushion (Figs. 1A, 1B).

MR imaging series of the liver were acquired at the 1.5T MAGNETOM Aera (Siemens Healthcare, Erlangen, Germany) using the 18-channel body flex coil (Fig. 1C). The optimized MR sequences were able to take into account the support table and immobilization devices, which neither interfered with, nor degraded the images.

A total of three sequences were systematically acquired:

- For T2 lesion visualization, axial series of Single Shot Fast Spin Echo T2-weighted with fat saturation (T2) were used. Image acquisition is triggered on exhale and allows motion artifact reduction. TR and TE are 5248 ms and 73 ms respectively.

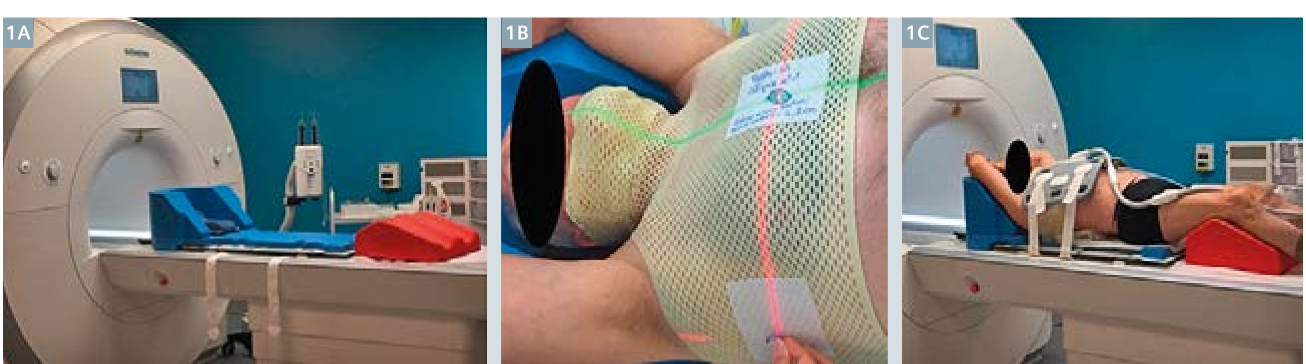


1 Dedicated table, supports and cushions for patient's immobilization and positioning at the MR 1.5T Aera scan **(1A)**; patient's thermo-plastic net with laser alignment **(1B)** and final setting with body coil ready for MR acquisitions **(1C)**.

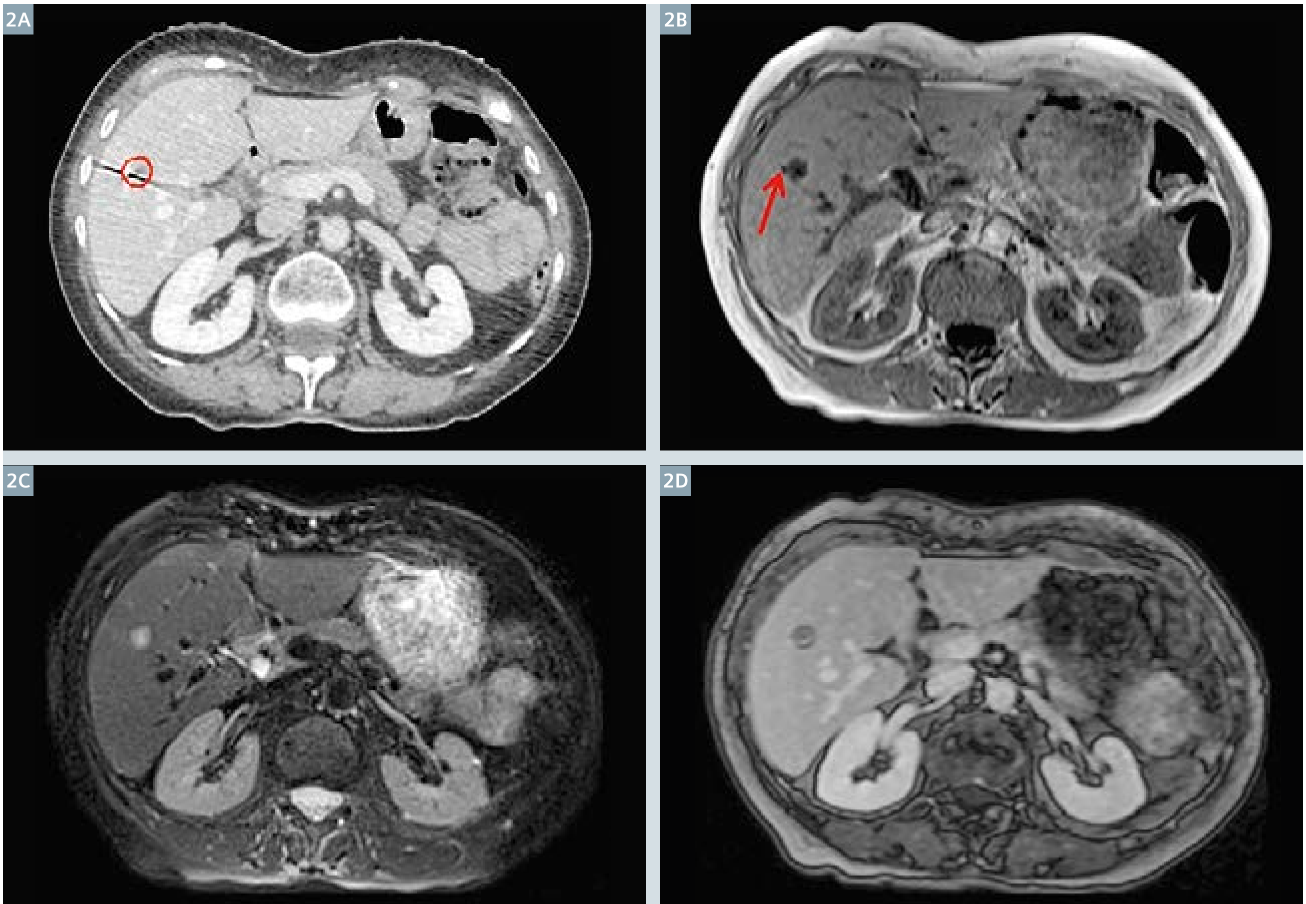


2 Example of registered image for a breast metastasis in liver segment V. Injected CT50 with target contour delineated in red thanks to the MR sequences **(2A)**, T1 Dixon with red arrow identifying fiducial **(2B)**, T2 showing hyper intense lesion **(2C)** and injected T1 TFL **(2D)**.

- The combination of Dixon and ultra-fast gradient echo T1-weighted images with CAIPIRINHA (Controlled Aliasing in Parallel Imaging Results in Higher Acceleration) technique allows performing the acquisition in one exhale breath-hold. Fiducials are visible on Dixon water separation images (T1 Dixon). TR and TE are 6.78 ms and 2.39 ms respectively.
- After injection of gadolinium-based contrast agent, lesion visualization was obtained with a T1-weighted Fast Low Angle Shot imaging sequence (T1 TFL) acquired using GRAPPA (Generalized Autocalibrating Partially Parallel Acquisitions) technique and with breath triggering on expiration phase. Gold fiducials are also visible on this sequence. TR and TE are 835 ms and 2.32 ms respectively.

Slice thickness was set to 2 mm for all series and pixel size was 1.48 x 1.48 mm² for T2 and T1 TFL; and 1.18 x 1.18 mm² for T1 Dixon. All sequences were acquired in the same plane and with the same slice positions in order to ease image registration in the treatment planning software.

The entire MR imaging protocol lasts generally between 15 and 20 minutes, depending on the regularity of the patient's breathing pattern.

## Image registration for treatment planning

Radiotherapy planning is based on a 4D CT reconstructed in six phases across the respiratory cycle, CT0 and CT50 corresponding to inhale and exhale phases respectively. The CT50 expiration phase is the image set used for MR image registration.

As the three MR image sets are registered, the T1 Dixon water-only image set is used to register to CT50 images using the gold fiducials and the two other sequences are automatically registered. T1 Dixon is useful to register water separation MR images based on fiducials' position, as they are the most visible on this sequence (see red arrow on Figure 2B). The two breath-triggered (expiration phase) sequences (T2 and injected T1 TFL) provide a motion artifact-free image necessary to accurately delineate the lesion (Figs. 2C, D). An example of lesion delineation is given in Figure 2A.

Target motion range is assessed based on fiducials' displacement. Treatment planning is most frequently performed on expiration phases, but when lesion movement caused by breathing is small, target contouring is done on all breathing phases based on fiducial movements, and treatment planning is achieved in free breathing.

## Conclusion

CT and MRI acquisitions in treatment position are performed with the same table and immobilization device. The use of MR imaging sequences optimized to account not only for the dedicated table and immobilization devices but also for fiducial visualization and tumor delineation allow high precision target delineation for treatment planning. The increasing number of patient cases eligible for SBRT and proof of its benefit have stimulated the effort to set up and improve new imaging protocols at our institute for a personalized and optimal SBRT treatment.

Recent developments in 4D MRI have demonstrated the possibility to sort and reconstruct the images according to the different phases of the respiratory cycle [4–7]. The use of 4D MRI acquisition would allow better registration with 4D CT planning over the entire breathing cycle. Delineation accuracy will benefit from significant improvements if the same respiratory phases are registered from both MR and CT modalities.

## Acknowledgments

The authors are thankful to Karen Mkhitaryan (Siemens Healthcare) for his help in setting up the MR image acquisition sequences.

### References

1 R. B. Case, J. J. Sonke, D. J. Moseley, J. Kim, K. K. Brock, L. A. Dawson, "Inter- and Intrafraction variability in liver position in non-breath-hold stereotactic body radiotherapy," Int. J. Radiat. Oncol. Biol. Phys., vol. 75, no. 1, pp. 302–308, 2009.

2 C. J. Haasbeek, F. O. Spoelstra, F. J. Lagerwaard, J. R. van Sörnsen de Koste, J. P. Cuijpers, B. J. Slotman, S. Senan, "Impact of Audio-Coaching on the Position of Lung Tumors," Int. J. Radiat. Oncol. Biol. Phys., vol. 71, no. 4, pp. 1118–1123, 2008.

3 Y. Seppenwoolde, H. Shirato, K. Katamura, S. Shimizu, M. van Herk, J. V. Lebesque, K. Miyasaka, "Precise and real-time measurement of 3D tumor motion in lung due to breathing and heartbeat, measured during radiotherapy," Int. J. Radiat. Oncol. Biol. Phys, vol. 53, no. 4, pp. 822–834, 2002.

4 M. von Siebenthal, G. Székely, U. Gamper, P. Boesiger, A. Lomax, P. Cattin, "4D MR imaging of respiratory organ motion and its variability," Phys. Med. Biol., vol. 52, no. 6, pp. 1547–1564, 2007.

5 C. Paganelli, P. Summers, M. Bellomi, G. Baroni, M. Riboldi, "Liver 4DMRI: A retrospective image-based sorting method.," Med. Phys., vol. 42, no. 8, pp. 4814–21, 2015.

6 K. B. Bernatowicz, R. L. Perrin, M. Peroni, D. C. Weber, A. J. Lomax, "4D-MRI: Future of Radiotherapy of Moving Targets?," MAGNETOM Flash, 62, vol. 2, pp. 74–76, 2015.

7 Z. Celicanin, O. Bieri, F. Preiswerk, P. Cattin, K. Scheffler, F. Santini, "Simultaneous acquisition of image and navigator slices using CAIPIRINHA for 4D MRI." Magn Reson Med. 2015 Feb;73(2):669-76.

## Contact

Soléakhéna Ken
Institut Universitaire du Cancer
Toulouse Oncopôle
1 avenue Irène Joliot-Curie
31059 Toulouse
France
ken.soleakhena@iuct-oncopole.fr

# Siemens Healthcare Publications

Our publications offer the latest information and background for every healthcare field. From the hospital director to the radiological assistant – here, you can quickly find information relevant to your needs.


**Medical Solutions**
Innovations and trends in healthcare. The magazine is designed especially for members of hospital management, administration personnel, and heads of medical departments.

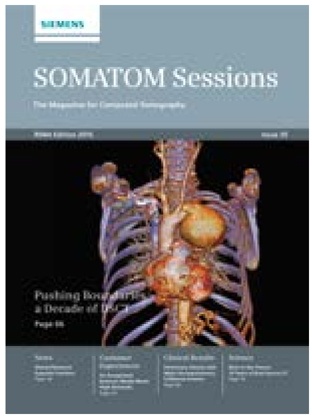


**SOMATOM Sessions**
Everything from the world of computed tomography.

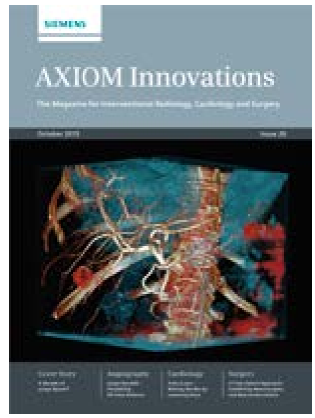


**AXIOM Innovations**
Everything from the world of interventional radiology, cardiology, and surgery.


**MAGNETOM Flash**
Everything from the world of magnetic resonance imaging.

MReadings – Imprint



Publisher:
**Siemens Healthcare GmbH**
Magnetic Resonance,
Karl-Schall-Straße 6, D-91052 Erlangen,
Germany

**Editor-in-chief:**
Antje Hellwich
(antje.hellwich@siemens.com)

**Editorial Board:**
Elena Nioutsikou; Heidrun Endt, M.D.;
Martin Requardt, Ph.D.; Zoltan Vermes;
Peter Kreisler, Ph.D.

**Production:**
Norbert Moser,
Siemens Healthcare GmbH

**Layout:**
Agentur Baumgärtner,
Friedrichstraße 4, D-90762 Fürth, Germany

**Printer:**
G. Peschke Druckerei GmbH,
Taxetstrasse 4,
D-85599 Parsdorf b. Munich,
Germany

Note in accordance with § 33 Para.1 of the German Federal Data Protection Law: Despatch is made using an address file which is maintained with the aid of an automated data processing system.

The statements and views of the authors in the individual contributions do not necessarily reflect the opinion of the publisher.

The information presented in these articles is for illustration only and is not intended to be relied upon by the reader for instruction as to the practice of medicine. Any health care practitioner reading this information is reminded that they must use their own learning, training and expertise in dealing with their individual patients. This material does not substitute for that duty and is not intended by Siemens Healthcare to be used for any purpose in that regard. The drugs and doses mentioned herein are consistent with the approval labeling for uses and/or indications of the drug. The treating physician bears the sole responsibility for the diagnosis and treatment of patients, including drugs and doses prescribed in connection with such use. The Operating Instructions must always be strictly followed when operating the MR system. The sources for the technical data are the corresponding data sheets. Results may vary.



We welcome your questions and comments about the editorial content of MAGNETOM Flash or MReadings. Please contact us at magnetomworld.med@siemens.com.

Manuscripts as well as suggestions, proposals and information are always welcome; they are carefully examined and submitted to the editorial board for attention. MAGNETOM Flash or MReadings is not responsible for loss, damage, or any other injury to unsolicited manuscripts or other materials. We reserve the right to edit for clarity, accuracy, and space. Include your name, address, and phone number and send to the editors, address above.

*MAGNETOM 7T is still under development and not commercially available yet. Its future availability cannot be ensured. This research system is not cleared, approved or licensed in any jurisdiction for patient examinations. This research system is not labelled according to applicable medical device law and therefore may only be used for volunteer or patient examinations in the context of clinical studies according to applicable law.

**Siemens Healthcare Headquarters**
Siemens Healthcare GmbH
Henkestr. 127
91052 Erlangen
Germany
Phone: +49 9131 84-0
siemens.com/healthcare

**Local Contact Information**
Siemens Medical Solutions USA, Inc.
40 Liberty Boulevard
Malvern, PA 19355-9998
USA
Phone: +1-888-826-9702
usa.siemens.com/healthcare

Order No. A91DI-MR-161225-P1-4A00 | Printed in USA 06-2016 | 

**siemens.com/healthcare**